



HAL
open science

Mutations in TTC29, Encoding an Evolutionarily Conserved Axonemal Protein, Result in Asthenozoospermia and Male Infertility

Patrick Lorès, Denis Dacheux, Zine-Eddine Kherraf, Jean-Fabrice Nsota Mbango, Charles Coutton, Laurence Stouvenel, Côme Ialy-Radio, Amir Amiri-Yekta, Marjorie Whitfield, Alain Schmitt, et al.

► To cite this version:

Patrick Lorès, Denis Dacheux, Zine-Eddine Kherraf, Jean-Fabrice Nsota Mbango, Charles Coutton, et al.. Mutations in TTC29, Encoding an Evolutionarily Conserved Axonemal Protein, Result in Asthenozoospermia and Male Infertility. *American Journal of Human Genetics*, 2019, 10.1016/j.ajhg.2019.10.007 . hal-02370384

HAL Id: hal-02370384

<https://hal.science/hal-02370384>

Submitted on 21 Dec 2021

HAL is a multi-disciplinary open access archive for the deposit and dissemination of scientific research documents, whether they are published or not. The documents may come from teaching and research institutions in France or abroad, or from public or private research centers.

L'archive ouverte pluridisciplinaire **HAL**, est destinée au dépôt et à la diffusion de documents scientifiques de niveau recherche, publiés ou non, émanant des établissements d'enseignement et de recherche français ou étrangers, des laboratoires publics ou privés.



Distributed under a Creative Commons Attribution - NonCommercial 4.0 International License

Mutations in *TTC29*, encoding an evolutionary conserved axonemal protein, result in asthenozoospermia and male infertility.

Patrick Lorès^{1,2,3}, Denis Dacheux^{4,5}, Zine-Eddine Kherraf^{6,7}, Jean-Fabrice Nsota Mbango^{1,2,3}, Charles Coutton^{6,8}, Laurence Stouvenel^{1,2,3}, Come Ialy-Radio^{1,2,3}, Amir Amiri-Yekta⁹, Marjorie Whitfield^{1,2,3}, Alain Schmitt^{1,2,3}, Caroline Cazin⁶, Maëlle Givelet^{1,2,3}, Lucile Ferreux¹⁰, Selima Fourati Ben Mustapha¹¹, Lazhar Halouani¹¹, Ouafi Marrakchi¹¹, Abbas Daneshpour⁹, Elma El Khouri^{1,2,3}, Marcio Do Cruzeiro^{1,2,3}, Maryline Favier^{1,2,3}, François Guillonnet^{1,2,3}, Marhaba Chaudhry^{1,2,3}, Zeinab Sakheli^{1,2,3}, Jean-Philippe Wolf^{1,3,10}, Catherine Patrat^{1,3,10}, Gérard Gacon^{1,2,3}, Sergey N. Savinov¹², Seyedeh Hanieh Hosseini¹³, Derrick R. Robinson⁴, Raoudha Zouari¹¹, Ahmed Ziyat^{1,2,3,10}, Christophe Arnoult⁶, Emmanuel Dulioust^{1,3,10}, Mélanie Bonhivers^{4,14}, Pierre F. Ray^{6,7,14} and Aminata Touré^{1,2,3,14*}.

¹ INSERM U1016, Institut Cochin, Paris 75014, France.

² Centre National de la Recherche Scientifique UMR8104, Paris 75014, France.

³ Faculté de Médecine, Université Paris Descartes, Sorbonne Paris Cité, Paris 75014, France.

⁴ Université de Bordeaux, Microbiologie Fondamentale et Pathogénicité, CNRS UMR 5234, Bordeaux, France.

⁵ Institut Polytechnique de Bordeaux, Microbiologie Fondamentale et Pathogénicité, UMR-CNRS 5234, F-33000 Bordeaux, France.

⁶ INSERM U1209, CNRS UMR 5309, Université Grenoble Alpes, 38000 Grenoble, France.

⁷ CHU de Grenoble, UM GI-DPI, Grenoble, F-38000, France.

⁸ CHU Grenoble Alpes, UM de Génétique Chromosomique, Grenoble, France.

⁹ Department of Genetics, Reproductive Biomedicine Research Center, Royan Institute for Reproductive Biomedicine, ACECR, Tehran-Iran

¹⁰ Laboratoire d'Histologie Embryologie - Biologie de la Reproduction - CECOS Groupe Hospitalier Universitaire Paris Centre, Assistance Publique-Hôpitaux de Paris. Paris 75014, France.

¹¹ Histologie Embryologie et Biologie de la Reproduction, Centre de Promotion des Sciences de la Reproduction. Polyclinique les Jasmins. Centre Urbain Nord. 1003. Tunis, Tunisia.

¹² Department of Biochemistry and Molecular Biology, University of Massachusetts, Amherst, Massachusetts 01003 USA.

¹³ Department of Andrology, Reproductive Biomedicine Research Center, Royan Institute for Reproductive Biomedicine, ACECR, Tehran-Iran

¹⁴ These authors contributed equally to this work

* Correspondence: aminata.toure@inserm.fr

Running title: *TTC29* mutations in MMAF and male infertility

Authors e-mail addresses

patrick.lores@inserm.fr
Denis.Dacheux@ipb.fr
ZEKherraf@chu-grenoble.fr
jfnsota@gmail.com
CCoutton@chu-grenoble.fr
laurence.stouvenel@inserm.fr
come.ialy-radio@inserm.fr
amir.amiriyekta@gmail.com
marjorie.whitfield@inserm.fr
alain.schmitt@inserm.fr
cazin.caroline@gmail.com
givelet.m@gmail.com
lucile.ferreux@aphp.fr
fourati_selima@yahoo.fr
halouani.l@planet.tn
marrakchiouafi@vivre.tn
adaneshi66@gmail.com
elma.el-khouri@hotmail.com
marcio.do-cruzeiro@inserm.fr
maryline.favier@inserm.fr
francois.guillonneau@parisdescartes.fr
chmarhaba@gmail.com
zeinabsaheli@hotmail.com
jean-philippe.wolf@aphp.fr
catherine.patrat@aphp.fr
gerard.gacon@orange.fr
ssavinov@umass.edu
h.hosseini313@yahoo.com
derrick-roy.robinson@u-bordeaux.fr
raouzou@gmail.com
ahmed.ziyyat@inserm.fr
christophe.arnoult@univ-grenoble-alpes.fr
emmanuel.dulioust@gmail.fr
melanie.bonhivers@u-bordeaux.fr
PRay@chu-grenoble.fr
aminata.toure@inserm.fr

Abstract

In humans, structural or functional defects of the sperm flagellum induce asthenozoospermia, which accounts for the main sperm defect encountered in infertile men. Herein we focused on Morphological Abnormalities of the sperm Flagellum (MMAF), a phenotype also termed “short tails”, which constitutes one of the most severe sperm morphological defects resulting in asthenozoospermia. In previous work based on whole exome sequencing of a cohort of 167 MMAF individuals, we identified bi-allelic loss of function mutations in over 30% of the tested subjects. In this study, we further analyzed this cohort and identified five individuals with homozygous truncating variants in *TTC29*, a gene preferentially and highly expressed in the testis, and encoding a Tetratricopeptide Repeat containing protein related to the intra flagellar transport (IFT). One individual carried a frameshift variant, another one carried a homozygous stop-gain variant and three carried the same splicing variant affecting a consensus donor site. The deleterious effect of this last variant was confirmed on the corresponding transcript and protein product. In addition, we produced and analyzed *TTC29* loss of function models in the flagellated protist *T. brucei* and in *M. musculus*. Both models confirmed the importance of *TTC29* for flagellar beating. We showed that in *T. brucei* the TPR structural motifs, highly conserved between the studied orthologs, are critical for *TTC29* axonemal localization and flagellar beating. Overall our work demonstrates that *TTC29* is a conserved axonemal protein required for flagellar structure and beating and that *TTC29* mutations are a cause of male sterility due to MMAF.

Keywords: Sperm, asthenozoospermia, MMAF, infertility, *TTC29*, TPR

Introduction

The mammalian sperm flagellum is an evolutionarily conserved organelle shaped on a microtubule-based cytoskeleton, called the axoneme, which also serves as the backbone of motile cilia¹. The core of the axoneme consists of nine peripheral doublets of microtubules surrounding a central pair of microtubules (CP), which confer the canonical (9+2) pattern. The peripheral doublets are connected to each another by the nexin-dynein regulatory complex; in addition, multiprotein T-shaped structures, called the radial spokes (RSs), connect each peripheral doublet to the central pair. Beating of motile cilia and flagella is governed by multiprotein ATPases complexes, called the outer and inner dynein arms (ODAs and IDAs, respectively), which are both harbored by the peripheral microtubules and drive the sliding of the peripheral microtubules responsible for flagellar movement². In contrast to motile cilia, the mammalian sperm harbors some peri-axonemal structures, such as the outer dense fibers (ODFs) and the longitudinal columns (LC), which associate to the axoneme nearly all along the flagellum³. In addition, a mitochondrial helix specifically surrounds the sperm axoneme in the midpiece region and is replaced by the fibrous sheath (FS) in the principal piece of the flagellum. These two accessory structures are, in particular, required for energy production^{4;5}.

Structural and/or functional defects of the sperm flagellum induce asthenozoospermia, which in humans is defined by reduced number or absence of motile spermatozoa in the ejaculate (<32% of progressive sperm), according to the World Health Organization reference values⁶. Asthenozoospermia may be associated with ciliary defects, as in Primary Ciliary dyskinesia (PCD [MIM 244400]), an autosomal recessive disease principally characterized by chronic airway infections^{7; 8} but is also evidenced in many infertile men with no other symptomatology (i.e. isolated asthenozoospermia). Overall asthenozoospermia is found with variable degrees of severity in more than 80% of infertile men⁹. Herein we focused on

isolated asthenozoospermia due to Multiple Morphological Abnormalities of the sperm Flagellum (MMAF), a phenotype also termed “short tails” or “stump tails”^{10; 11}, which constitutes one of the most severe sperm morphological defects leading to male sterility¹². MMAF is defined by the presence of a mosaic of sperm cells with absent, short, irregular and coiled flagellum, associated with a severe disorganization of the peri-axonemal structures such as dysplasia of the fibrous sheath^{10; 11}. The proportion of these anomalies is variable between MMAF individuals but all are constantly present at frequencies largely exceeding those found in fertile men¹³.

In the last five years, high-throughput genetic investigations of MMAF individuals from various ethnical origins, allowed the rapid identification of a dozen genes, whose loss-of-function caused by biallelic variants account for over one third of the MMAF cases. Hence frequent mutations were identified in *DNAH1* (MIM:603332)¹⁴⁻¹⁶, *DNAH2* (MIM 603333)¹⁷, *CFAP43/WDR96* (MIM:617558)^{18; 19}, *CFAP44/WDR52* (MIM:617559)¹⁸⁻²⁰, *CFAP69* (MIM:617949)²¹, *CFAP251/WDR66* (MIM:618146)^{22; 23}, *FSIP2* (MIM:615796)²⁴, *ARMC2* (MIM:618424)²⁵, *QRICH2* (MIM:618304)²⁶, *TTC21A* (MIM:611430)²⁷ and *SPEF2* (MIM:610172)²⁸ in unrelated MMAF subjects. In addition, mutations in *CFAP65* (MIM:614270)¹⁹, *CEP135* (MIM:611423)²⁹ and *AK7* (MIM:615364)³⁰ were reported in single familial MMAF cases. With the aim to identify additional genetic causes of human asthenozoospermia related to MMAF, we further analyzed whole exome sequencing data from a cohort of 167 MMAF individuals previously established by our team²⁵ and report the identification and characterization of *TTC29* bi-allelic truncating mutations in five unrelated individuals. In addition, by performing *in silico*, *in vitro* and *in vivo* studies, using *T. brucei* and *M. Musculus* mutant models, we demonstrate that *TTC29* is a conserved axonemal protein required for correct flagellar beating and motility. in three evolutionary distant species.

Material and methods

Study Participants and Whole Exome Sequencing (WES)

We analyzed data obtained by WES performed for a total of 167 men affected by primary infertility associated with a MMAF phenotype²⁵. WES and bioinformatics analyses were performed according to our previously described protocol using the human genome assembly GRCh38 as a reference sequence¹⁸. All the recruited individuals displayed isolated infertility with no other clinical features; in particular, primary ciliary dyskinesia (PCD) syndrome was excluded. In this cohort, 83 individuals originated from North Africa (mainly from Algeria, Libya and Tunisia) and sought consultation for primary infertility at the “Clinique des Jasmins” in Tunis, 52 individuals originated from the Middle East (Iran) and were treated in Tehran at the Royan Institute (Reproductive Biomedicine Research Center) for primary infertility, and 32 individuals were recruited in France, mainly at the Reproductive Department at Cochin Hospital in Paris. All individuals presented with a typical MMAF phenotype, which is characterized by severe asthenozoospermia (total sperm motility below 10%; normal value over 40% according to the World Health Organization reference values⁶, in association with increased level of the following sperm flagellar abnormalities : short, absent, coiled, bent, or irregular flagella, in comparison with the normal ranges observed in control fertile individuals¹³.

Informed consent was obtained from all the individuals participating in the study according to local protocols and the principles of the Declaration of Helsinki. The study was approved by local ethics committees, and samples were then stored in the CRB Germethèque (certification under ISO-9001 and NF-S 96-900) according to a standardized procedure or were part of the

Fertithèque collection declared to the French Ministry of Health (DC-2015-2580) and the French Data Protection Authority (DR-2016-392).

Sanger sequencing

The selected mutations in *TTC29* were validated by Sanger sequencing performed on ABI 3130XL (Applied Biosystems); analyses were performed using SeqScape software (Applied Biosystems). Sequences of primers used and expected product sizes are summarized in Table S2.

Semen analysis

Semen samples were obtained by masturbation after a period of two to seven days of sexual abstinence. Semen samples were incubated at 37°C for 30 minutes for liquefaction; ejaculate volume and pH, sperm concentration, vitality, morphology and motility were evaluated according to World Health Organization (WHO) guidelines⁶. Sperm vitality was assessed by eosin staining, and sperm morphology was analysed on Schorr stained semen smears according to David's classification³¹.

Transmission Electron Microscopy analysis of sperm cells

Human or mouse sperm cells (10 millions) were fixed by incubation in 0.1 M phosphate buffer pH 7 supplemented with 3% glutaraldehyde (Grade I; Sigma-Aldrich Co. Saint-Louis, MO, USA) for 2 h at room temperature. The samples were washed twice in PBS and resuspended in 0.2 M sodium cacodylate buffer. The samples were then post-fixed by incubation with 1% osmium tetroxide (Electron Microscopy Sciences, Hatfield, UK), after which they were dehydrated by immersion in a graded series of alcohol solutions and embedded in Epon resin (Polysciences Inc., Warrington, USA). Semi-thin sections were cut and stained with toluidine blue-Azur II. Ultra-thin sections (90 nm) were cut with a Reichert

Ultracut S ultramicrotome (Reichert-Jung AG, Wien, Austria) and were then stained with uranyl acetate and lead citrate. Sections were analyzed with a JEOL 1011 microscope and digital images were acquired with a Gatan Erlangshen CCD camera and Digital Micrograph software.

RT-PCR analysis of human sperm cells

200-800 ng of total RNA were extracted from 5-10 millions of human spermatozoa using NucleoSpin RNA kit (Macherey Nagel, Düren, Germany) and subjected to reverse transcription with High-Capacity cDNA Reverse Transcription kit (Applied Biosystems, Fisher Scientific, Hampton, NH, USA) following the manufacturer's instructions. PCR reactions were performed with GoTaq® DNA polymerase (Promega, Madison, WI, USA) using *TTC29* specific primers. Amplicons were gel purified and sequenced (Eurofins Genomics, Les Ulis, France). Sequences of primers used and expected product sizes are summarized in Table S3.

Western blot analysis on sperm cells or testis extracts

Denaturated protein samples corresponding to equal amounts of spermatozoa (from human or mouse) or mouse testis extracts were loaded on SDS-PAGE (12% acrylamide/bisacrylamide (40% 37.5:1)) and transferred onto nitrocellulose membranes. The membranes were blocked in 5% milk in PBS-Tween 0.1% or 3% BSA in TBS-Tween 0.1%, and immunoblot analysis was performed using the indicated primary antibodies. Details of antibodies and dilutions used for western blot assays are provided in Table S4.

Immunofluorescence analysis of sperm cells

10 µl of semen samples were spread onto a Superfrost Plus slide (Menzel Glasbearbeitungswerk, GmbH & Co. KG, Braunschweig, Germany). Sperm was fixed by incubation with PBS/4%

paraformaldehyde for 10 minutes. The slides were incubated 20 minutes at 95°C in citrate buffer (H-3300, VectorLabs, Burlingame, CA, USA). The slides were next treated with 0.2% Triton in PBS for permeabilization and then blocked by incubation in 1% BSA for 1 hour. They were then incubated with primary antibodies for 2 hours at room temperature and then secondary antibodies for one hour at room temperature. The slides were mounted in Vectashield medium (Vector Laboratories, Burlingame, USA) supplemented with 0.5 µg/ml DAPI. Slides were analyzed with a Zeiss Axiophot epifluorescence microscope. Digital images were acquired with a cooled charge-coupled device (CCD) camera (Hamamatsu Co. Japan), under identical instrument settings, with MetaMorph® software (Molecular Devices, Inc. USA). Details of antibodies and dilutions used for immunofluorescence assays are provided in Table S4.

CRISPR mutant mouse engineering

Handling of mice and experimental procedures were performed in accordance with institutional and national guidelines for the care and use of laboratory animals. Authorizations were obtained from local and governmental ethical review committees: Authorization APAFIS #14124-2017072510448522 v26, Touré (2018-2025). *TTC29* mutant mice were generated by the “Transgenesis and Homologous Recombination” core facility of the Institut Cochin (INSERM U1016, Paris, France), using CRISPR/Cas9 technique. The RNA guide targeting *Ttc29* exon 5, 5'-CAAAGGGCTGTTCGAAAGAAG-3', was designed using CRISPOR selection tool (<http://crispor.org>). gRNA was pre-incubated with Cas9 protein (RT, 10 min) to obtain functional ribonucleoprotein (RNP) complexes. The final injection mix containing 0.6 µM of gRNA and Cas9 protein (1.5 µM) in TE-0.1 buffer (10mM Tris-HCl, 0.1mM EDTA), has been injected into 210 fertilized oocytes of superovulated C57BL/6JRj females. 92 typical 2-cell stage embryos were subsequently implanted into the oviduct of 5 pseudo-pregnant B6CBAF1 females. Subsequent genotyping of CRISPR edited founders was performed by PCR amplification (GoTaq® DNA

Polymerase, Promega, Madison, WI, USA) on DNA extracted from tail biopsies (NucleoSpin® Tissue, Macherey-Nagel, Düren, Germany) and PCR-product sequencing (Eurofins Genomics, Les Ulis, France). Sequences of primers used and expected product sizes are summarized in Table S5. Mice carrying *Ttc29* mutational events were bred with C57BL6/JRj mice to ensure germline transmission and eliminate any possible mosaicism.

Mouse sperm morphological analysis

Spermatozoa were retrieved from cauda epididymes in PBS buffer and spread onto a Superfrost Plus slide (Menzel Glasbearbeitungswerk, GmbH & Co. KG, Braunschweig, Germany). Sperm cells were fixed by incubation with PBS/4% paraformaldehyde for 10 minutes and stained following Papanicolaou protocol (Hematoxylin, OG6, EA50).

Mouse sperm motility analysis

Sperm motility was assessed by Computer Aided sperm Analysis (CASA) using CEROS II apparatus (Hamilton Thorne, Beverly, MA USA). Briefly, mouse sperm cells expelled from the cauda epididymis were recovered into M2 medium (Sigma-Aldrich, Saint-Louis, MO, USA). The movements of at least 500 sperm cells per sample were analyzed in 20 µm chambers (Leja Products B.V., Netherlands) with Zeiss AX10 Lab. A1 microscope (10x objective), using HT CASAI software.

The settings were as follows: acquisition rate, 60 Hz; number of frames, 45; minimum head brightness, 175; minimum tail brightness, 80; minimum head size, 10 µm²; minimum elongation gate, 1%; maximum elongation gate, 100%; objective magnification factor, 1.2.

The principal motility parameters measured were: curvilinear velocity (VCL), average path velocity (VAP), straight-line velocity (VSL), beat/cross frequency (BCF), amplitude of lateral

head displacement (ALH). Progressive sperm cells were characterized by average path velocity (VAP) $>45\mu\text{m/s}$ and straightness ($\text{STR}=\text{VSL}/\text{VAP}$) $>45\%$, respectively.

Gamete preparation and *in vitro* fertilization

Oocyte preparation: C57BL6/J female mice of 6-8 weeks-old (JANVIER LABS, France) were superovulated with 5 IU of pregnant mare serum gonadotropin (PMSG) and 5 IU human chorionic gonadotropin (hCG) (Intervet, France) 48 hours apart. About 14 hours after hCG injection, the animals were sacrificed by cervical dislocation. Cumulus oophorus were collected by tearing the ampulla wall of the oviduct, placed in Fercult medium (FertiPro N.V, Belgium) supplemented with 3% BSA (Sigma–Aldrich), and maintained at 37°C under 5% CO₂ in air under mineral oil (Sigma–Aldrich). When experiments were performed with zona pellucida (ZP)-free oocytes, cumulus cells were removed by a brief exposure to hyaluronidase IV-S (15 mg/ml, Sigma–Aldrich). The ZP was then dissolved with acidic Tyrode's (AT) solution (pH 2.5) (Sigma–Aldrich) under visual monitoring. The zona-free eggs were rapidly washed five times and kept at 37°C under 5% CO₂ in air for 2 to 3 hours to recover their fertilization ability.

Capacitated sperm preparation: mouse spermatozoa were obtained from the cauda epididymides of C57BL6/J male mice (8 to 10-week-old) and capacitated at 37°C under 5% CO₂ for 90 minutes in a 500 μl drop Fercult medium supplemented with 3% BSA, under mineral oil.

In vitro fertilization: cumulus-intact and zona-free eggs were inseminated with capacitated spermatozoa for 3 hours in a 100 μl drop of Fercult medium 3% BSA at a final concentration of 10⁶ or 10⁵ per ml, respectively. Then, they were washed and directly mounted in Vectashield/DAPI (Vector laboratories, CA, USA) for observation under UV light

(Nikon Eclipse E600 microscope). Only oocytes showing at least one fluorescent decondensed sperm head within their cytoplasm were considered fertilized and according to this the fertilization rate per cumulus-intact (FR) was evaluated. To assess the fertilization index (FI), the number of decondensed sperm heads per zona-free oocyte was recorded.

Mice Breeding Assay

To test the fertility, three pubescent *Ttc29*^{-/-} (L5 or L3 lines) and 5 wild-type littermates, aged of 8 weeks, were mated each with two C57BL/6 J female mice, during a 4-month period. The number of pups per litter and the number of litters per female were recorded throughout the breeding assay period.

***Trypanosoma brucei* culture and transfection**

The trypanosome cell lines used in this study derived from the procyclic parental form *T. brucei* SmOxP427 strain, co-expressing the T7 RNA polymerase and the tetracycline repressor³². Cells were cultured at 27°C in SDM79 medium containing 10% (v/v) heat-inactivated foetal calf serum, 10 µg/ml hemin, supplemented with puromycin (1 µg/ml), and transfected as previously described³³ using specific transfection buffer³⁴, and cloned by serial dilution. The culture medium was supplemented, when required, with blasticidin (10 µg/ml), neomycin (10 µg/ml), and phleomycin (5 µg/ml). RNA interference (RNAi) was induced with tetracycline (10 µg/ml).

***Trypanosoma brucei* cell lines generated for this study**

For RNAi, a fragment of the *TbTTC29* ORF was amplified by PCR (bp 352-806, corresponding to amino acids 118-268) and cloned between the *Xho*I and *Xba*I sites of p2T7tiB. SmOxP427 cells were transfected with the *Not*I-linearized plasmid. After selection, several clones were analysed and one clone was chosen for further studies (cell line RNAi^{*TbTTC29*}). To produce an endogenous

TbTTC29 with a carboxy-terminal 10TY1 epitope-tag³⁵, RNAi^{*TbTTC29*} cells were transfected with a tagging cassette that was obtained by PCR using the pPOTv7-blast-10xTY1 as a template (cell line *TbTTC29::TY1/RNAi^{TbTTC29}*). A similar approach was used to generate a cell line expressing *TbTTC29-Nter::myc* (aa 1-120 of *TbTTC29*) in the *TbTTC29::TY1/RNAi^{TbTTC29}* background, using the pPOTv7-10myc-neomycin vector as a template (cell line *TbTTC29::TY1/TbTTC29-Nter::myc/RNAi^{TbTTC29}*). Sequences of primers used and expected product sizes are summarized in Table S6.

Immunofluorescence analysis of *Trypanosoma brucei*

Cells were collected, washed, and processed for immunolabelling on methanol fixed detergent-extracted cells (cytoskeleton, CSK) as previously described³⁶. Cytoskeletons were incubated 1 hour at RT with primary antibodies and then with secondary antibodies. Nuclei and kinetoplasts were stained with DAPI (10 µg/ml). Images were acquired on a Zeiss Imager Z1 microscope, using a Photometrics Coolsnap HQ2 camera, with a 100X Zeiss objective (NA 1.4) using Metamorph software (Molecular Devices), and processed with ImageJ.

Trypanosoma sedimentation assays and video-microscopy

Sedimentation assays were performed as previously described³⁷. Briefly, the cultures of parental (WT), non-induced and RNAi-induced cells were placed in cuvettes at a density of 1.10^7 cells/ml and incubated another 24 h without shaking. The optical density at 600nm (OD) was then measured before mixing (ODb, the cell density reflecting the “swimming” cells) and after mixing (ODa, the cell density reflecting “swimming” and “sedimenting” cells). The graphs represent the percentage of sedimentation calculated as $100 - (ODb/ODa) \times 100$ and normalized with the parental cells. Video-microscopy was carried out as previously described³⁸. Briefly, parental cells and 8-days-RNAi induced cells were washed in

PBS. Cellular mobility was recorded by phase contrast on a Zeiss AxioImager Z1 with a 40x lens (NA 1.3). Twenty-five seconds of digital video from separate regions were captured and analysed using MetamorphH software (Molecular Devices).

Western-blotting analysis on *Trypanosoma brucei* cells

Proteins from whole cell extracts ($5 \cdot 10^6$ cells per well) or from subcellular fractions (cytoskeleton or flagellum) were separated on 12% SDS-PAGE and semi-dry transferred (BioRad) for 45 min at 25V on PVDF membrane. After a 1 hour-blocking step in 5% skimmed milk in TBS-0.2% Tween-20 (blocking solution, BS), the membranes were incubated overnight at 4°C with the primary antibodies in BS. After 10-min washes in BS, then 1M NaCl, then BS, the membranes were incubated with the HRP-conjugated secondary antibodies, washed twice 10 min in blocking buffer and twice 5 min in TBS. Blots were revealed using the Clarity Western ECL Substrate kit (Bio Rad) on a ImageQuant LAS4000 apparatus and quantified using ImageJ. Stripping of the membranes was performed when required by incubation in glycine 100mM pH3, SDS 1%, NP40 0.1% (2x 10 min), followed by 3 washes in TBS; the membranes were then blocked in BS and incubated as described above with another primary antibody.

Statistical analysis

Results are expressed as mean \pm SEM of at least three independent experiments. The following statistical tests were performed, when appropriated: one-tailed unpaired t-tests, one-way ANOVA followed by Tukey's test, and Chi-squared tests t. Results were analyzed in GraphPad Prism version 7.00 for Windows, GraphPad Software, La Jolla California USA,

www.graphpad.com. Differences were considered as statistically significant when p-value < 0.05.

Results

Identification of *TTC29* bi-allelic truncating variants in MMAF infertile individuals

Whole Exome Sequencing (WES) data from a cohort of 167 MMAF individuals were analyzed in order to identify new candidate genes for severe asthenozoospermia. Previous analyses of this cohort permitted to identify bi-allelic variants in a total of 58 men (35%) in confirmed MMAF associated genes (*DNAH1*, *CFAP43*, *CFAP44*, *CFAP69*, *WDR66*, *FSIP2*, *ARMC2*, *TTC21* and *SPEF2*)^{21; 25; 27; 28}. We therefore consider that the cause of the MMAF phenotype is established for these 58 men, leaving 109 undiagnosed individuals. In these remaining undiagnosed individuals, we identified *TTC29* (Tetratricopeptide repeat domain 29; Gene ID: 83894) as a very good candidate since five unrelated individuals presented a homozygous truncating variant in this gene. *TTC29* is located on chromosome 4 and contains 13 exons (ENST00000325106; RefSeq transcript NM_031956.3), predicting a 475-amino-acid protein (UniProtKB: Q8NA56). The *TTC29* protein comprises five tetratricopeptide repeats (TPR), which are 34 amino acid repeats present in a wide variety of proteins, forming alpha-helices that behave as scaffolds for protein-protein interactions and assembly of multiprotein complexes³⁹⁻⁴¹. Based on public tissue expression databases (EMBL-EBI Expression Atlas; NCBI and GTEx), *TTC29* is found to be highly expressed in the testis and, to a much lesser extent in the lung. Quantitative single-cell RNA sequencing datasets from human adult testis (ReproGenomics Viewer)^{42; 43} indicate an expression in the germ cells from zygotene spermatocyte to late spermatid stage but not in the testicular somatic cells (i.e. Leydig and Sertoli cells), strongly suggesting a role in sperm cells differentiation and/or function. In addition, the *TTC29* protein was positively detected in human sperm proteome⁴⁴ whereas it was near absent in human airway cilia⁴⁵. Among the five *TTC29* mutated individuals, two originated from North Africa, one from central Africa (Niger) and two from Iran. The three African subjects (*TTC29*₁, *TTC29*₂ and *TTC29*₃) were homozygous for the

same variant c.176+1G>A (p.Tyr60*). This variant alters the canonical donor splice site of *TTC29* exon 4 and was identified in gnomAD at a frequency of 3.42e-4. The two remaining Iranian individuals carried two different truncating variants. Individual TTC29_4 was homozygous for a five nucleotide deletion, c.330_334delGGAGG (p.Glu111Alafs*), which was found in gnomAD at a frequency of 1.21e-5, and individual TTC29_5 was homozygous for the c.750C>A (p.Tyr250*) variant, absent from the gnomAD database. These two variants are deleterious as they induce a premature stop codon (positions 113 and 250, respectively, in the 475-amino acid *TTC29* protein sequence). The presence of all *TTC29* homozygous variants was confirmed by Sanger sequencing on DNA samples from the five individuals, as illustrated in **Figure 1A**, and the consequences of the variants on protein translation are shown in **Figure 1B**.

Lack of *TTC29* protein in sperm from individual TTC29_1, carrying the c.176+1G>A mutation

All three *TTC29* identified variants are predicted to introduce a premature stop codon in the first half of the protein sequence, therefore potentially inducing mRNA decay and if not, a truncated protein, which would lack most of the TPR functional domains. In order to provide further arguments for the pathogenicity of the identified variants, we analyzed the transcript and levels of protein in semen samples available from individual TTC29_1 carrying the c.176+1G>A mutation, which affects exon 4 consensus splice donor site. We first amplified *TTC29* transcripts in sperm cells from control individual and individual TTC29_1, using primers located in exons 3 and 5. The levels of *TTC29* transcripts were reduced in sperm cells from individual TTC29_1, as compared to what was observed in a control individual while the expression levels of *HPRT* (an ubiquitous housekeeping gene) was similar in both individuals (**Figure 1C**), indicating that the mutated transcript was subject to incomplete mRNA decay.

Sanger sequencing of the amplified transcript showed an abnormal exon 4/5 boundary with an additional 19 nucleotides retained from intron 4, inducing a premature stop codon one nucleotide after the end of exon 4 (**Figure 1C**). We then performed western blot experiments using two different antibodies raised against TTC29: antibody Ab73, binding amino acids 9-92 (N-terminus) and antibody Ab06, binding amino-acids 174-260 (middle region). When using antibody Ab73, the TTC29 protein was detected at the predicted molecular weight of 55 kDa in sperm protein extracts from the control individual but no protein was observable in sample from individual TTC29_1, whereas Lamin, a component of the nuclear membrane, was equally detected in samples from both individuals (**Figure 1D**). Similar results were observed when using the antibody Ab06, although the signal intensity was much lower (**Figure S1A**). To confirm these results, we performed immunodetection assays using antibody Ab73; we observed that the TTC29 protein was detected along the sperm flagellum of the control individual but absent in sperm cells from individual TTC29_1, which were able to assemble a flagellum as visualized by α -Tubulin staining (**Figure 1D; Figure S1B**). Taken together, the results confirm the deleterious effect of the c.176+1G>A splice mutation, which results in the total absence of TTC29 protein in sperm from individual TTC29_1.

Phenotypical characterization of MMAF individuals harboring *TTC29* truncating variants

All five individuals harboring *TTC29* truncating mutations had a normal somatic karyotype (46, XY) with normal bilateral testicular size, hormone levels, and secondary sexual characteristics. Semen analysis revealed normal vitality and normal sperm number, except for individual TTC29_1 who showed a moderate decrease of sperm number (16.8 millions; normal value: 39 millions) (**Table 1**). All five individuals presented with severe asthenozoospermia, with nearly zero progressive spermatozoa present in the ejaculate

(between 0 and 2%; normal value >32%) and less than 10% of total motile spermatozoa (normal value >40%) (**Table 1**). In addition, no spermatozoa with normal morphology were recorded (0% typical forms; normal value >23%) for any of the five individuals. As illustrated for individual TTC29_1 (**Figure 2A**), quantitative sperm morphological analysis confirmed a typical MMAF phenotype defined by sperm with absent, short and irregular flagella in rates largely exceeding the distribution ranges observed in control fertile men¹³ (**Table 1**). In addition, the global average of semen parameters from the five individuals carrying mutations in *TTC29* was found similar to that of the other MMAF individuals from the cohort with known or unknown genetic causes (**Table 2**). Ultrastructure analysis of the sperm cells from individual TTC29_1 was performed by transmission electron microscopy (TEM) and showed abnormal midpiece and fibrous sheath together with severe axonemal disorganization (**Figure 2B**), as previously described for MMAF individuals. Quantification on a total number of 23 transversal sections of sperm cells from individual TTC29_1, indicated 36% of abnormal axonemal structure including 27% of sections lacking the central pair (9+0 pattern) and a few sections displaying global microtubule doublets disorganization (**Figure 2B**). The percentage of sections with axonemal defects observed in sperm from individual TTC29_1 (36%) was however much lower than what was previously reported for MMAF individuals carrying mutations in *CFAP43* and *CFAP44*, also encoding axonemal proteins (95% in average including 81.8 % and 66.7% of sections lacking the central pair, respectively)¹⁸. Despite this observation, we could confirm the extent of the axonemal anomalies, as immuno-marking of SPAG6, a component of the central pair complex, gave nearly no signal in sperm from individual TTC29_1 (**Figure 2C**). In addition, although positive, immunodetection with a set of antibodies specifically marking other functional protein complexes of the axoneme, such as the ODAs (DNAI1), IDAs (DNALI1) and RSs (RSPH1), appeared weaker than the patterns obtained in sperm from control individuals (**Figures S2, S3**) while FS staining with AKAP4

antibody was unaffected (**Figures S2, S3**). Overall, this indicated that the absence of TTC29 had a strong impact on the positioning of other axonemal proteins.

Phenotypical characterization of CRISPR-engineered mice lacking TTC29 protein

In mouse, *Ttc29* is located on chromosome 8 and contains 14 exons predicting a 471-amino-acid protein (UniProtKB: Q80VM3; NP_898919.3), which share 75% of identity with human TTC29 protein. Similar to humans, information retrieved from public expression databases and from the literature⁴⁶ indicate a strong expression of *Ttc29* in rodent testis and germ cells, which prompted us to further investigate the mouse orthologue. Using the CRISPR-Cas9 technique, we generated and characterized two different mouse lines, *Ttc29* L5 and L7, with mutational events targeting *Ttc29* exon 5, comparable to the region mutated in individual TTC29₁. The mutations generated in *Ttc29* L5 and L7 mouse lines corresponded to a 1 nucleotide-insertion and 17 nucleotide-deletion, respectively, and were both expected to induce a translational frameshift and the production of a truncated protein, if any (**Figure S4A,C**). Heterozygous mutant animals of L5 and L7 mutant lines were mated to generate homozygous offspring, which were obtained at the expected Mendelian frequencies of 26.3% (n=81) and 22.7% (n=68) for L5 and L7, respectively, thus excluding embryonic or perinatal lethality due to *Ttc29* mutations. We first validate the mutant mouse models by performing western blot experiments on testes protein extracts from *Ttc29* L5 and L7 homozygous mutant mice, which indicated the absence of TTC29 protein and of any truncated protein (**Figure S4B**). To confirm this result, we prepared purified sperm flagella preparations from wild-type versus mutant mice, following previously described protocols⁴⁷, and performed tandem mass spectrometry (MS/MS) analysis. TTC29 peptides were readily identified in wild-type sperm preparations (**Table S6**), confirming that in the mouse TTC29 protein also locate to the flagellum. However, no peptides from TTC29 protein could be recovered from the mutant

samples (n=4), therefore formally excluding the production of a truncated protein, similar to what was observed in individual TTC29₁ carrying the c.176+1G>A mutation (**Table S1**). We next analyzed the phenotype and the male reproductive functions of *Ttc29* L5 and L7 homozygous mutant males. Both mutant males were viable and indistinguishable from their wild-type littermates in survival rate and general appearance. Normal body, testes and epididymides weights were also reported (**Table 3**). Histological analysis indicated normal cytoarchitecture of the testes and epididymides. In addition, all stages of germ cells differentiation were observed within the seminiferous tubules of the testes, indicating that spermatogenesis occurred normally in those mutant animals (**Figure S5, S6**). In consistence with this, no increase in germ cells apoptosis was detected in seminiferous tubules of *Ttc29* mutant testes (**Figure S7**) and epididymal sperm count were normal (**Table 3**). Importantly, *Ttc29* mutant sperm did not display a typical MMAF phenotype and appeared overall normal in length (**Figure 3A**). A significant increase in more subtle morphological defects of the flagellum was however observed in comparison with wild-type mice (**Table 3**). In particular *Ttc29* L5 and *Ttc29* L7 sperm flagella sometime displayed a disjunction at midpiece-principal piece junction, a folding concerning this same region and an increase of flagella with irregular caliber (L5: 7.52% and L7: 6.00% compared to wild type: 3.48%; p values <0.01 and 0.05, respectively) (**Figure 3A**). Ultra-structural analyses performed by TEM indicated an increased number of transversal sections with an abnormal axonemal organization such as supernumerary or missing outer microtubule doublets and global microtubule disorganization (**Figure 3B**). Similar to sperm from individual TTC29₁, we performed immunofluorescence detection of DNAI1, DNALI1, RSPH1 and SPAG6 axonemal proteins in sperm from *Ttc29* mutant mice but we did not observe obvious differences compared to wild-type (data not shown). Furthermore, we analyzed the label free quantification intensity of DNAI1, DNALI1, RSPH1 and SPAG6 peptides, which we identified by MS/MS analyses on flagellum fractions

from wild-type and mutant *Ttc29* mice and did not observe statistically significant changes between the two genotypes (**Table S7**). Overall, this confirmed that in contrast to sperm from individual TTC29_1, the DNAI1, DNALI1, RSPH1 and SPAG6 proteins are present in sperm from *ttc29* mutant mice, which is somewhat consistent with their minor axonemal defects. Importantly, while the percentages of viable and total motile sperm in *Ttc29* mutant mice were normal, the fraction of progressive sperm was reduced (**Table 3; Figure S8**) and detailed assessment of the sperm kinematic parameters by means of computer assisted sperm analysis (CASA) confirmed a severe alteration of sperm velocity and flagellar beating. The curvilinear velocity (VCL), the straight-line velocity (VSL) and the average-path velocity (VAP), which are three kinematics assessing sperm velocity, were strongly diminished in *Ttc29* mutant sperm (**Figure 4A; Figure S8**). The beat/cross frequency (BCF), which is a measure of flagellar beating was also found slightly decreased in *Ttc29* mutant sperm while the head movements assessed by the amplitude of lateral head displacement (ALH) were unaffected (**Figure 4A**). Notably, when sperm from *Ttc29* L5 and L7 mutant mice were capacitated *in vitro*, they displayed the normal associated-tyrosine protein phosphorylation (**Figure S9**) but were not efficient in fertilizing intact or ZP-free oocytes collected from wild type females (**Figure 4B**). Hence the fertilization rates (FR; percentage of fertilized oocytes), of *Ttc29*^{-/-} L5 and L7 sperm were of 5.56 ± 0.03 and 5.74 ± 0.03 , respectively, compared to 32.71 ± 0.05 for controls sperm ((mean \pm SEM), p values <0.01 and 0.001). Similarly, the fertilization index (FI; mean number of male nuclei per oocyte) of *Ttc29* L5 and L7 mutant sperm were severely diminished and of 0.64 ± 0.08 and 0.55 ± 0.09 , respectively, compared to 1.10 ± 0.11 for control sperm (mean \pm SEM), p values <0.01 and 0.001). In line with these results, when *Ttc29* L5 and L7 mutant males were mated with wild-type females, they produced litters reduced in size and number, in comparison with their control littermates (**Figure 4C**). The number of pups per litter during a breeding period of 124 days was

3.57±0.65 and 4.00±0.71 for *Ttc29*^{-/-} L5 and L7 males as compared to 6.50±0.41 for control males (**Figure 4C**). In addition, over the same breeding period, the number of litters per female breeder crossed with *Ttc29*^{-/-} L5 and L7 males was 1.17±0.48 and 0.67±0.21, in comparison with 3.40±0.27 for control males (**Figure 4C**). Overall, we demonstrated that in the mouse, *Ttc29* homozygous loss of function is associated with minor morphological and ultra-structural defects of the sperm flagella while it results in a profound alteration of sperm flagellar velocity and beating frequency, strongly impairing fertilization, both *in vitro* and *in vivo*.

Localization of TTC29 orthologue protein in *T. brucei* flagella

In order to further assess the importance of the TTC29 protein in flagellar beating, we chose to investigate the localization and function of its orthologue in *Trypanosoma brucei* (*T. brucei*), a flagellated protozoan, which has largely contributed to elucidating the molecular pathogeny of human ciliopathies⁴⁸. The *T. brucei* axoneme is similar to that of mammalian sperm flagella but its para-axonemal structure, although comparable in function, is different. In *T. brucei*, the sperm FS and ODFs present in mammalian flagella, are replaced by the paraflagellar rod (PFR), a complex structure connecting with axonemal doublets (4–7)⁴⁹. The PFR plays a role in flagellum motility^{50; 51} and serves as a platform for metabolic and signaling enzymes⁵²⁻⁵⁴. By performing BlastP analysis on the *T. brucei* genome database⁵⁵ using the human TTC29 protein sequence, we identified the *T. brucei* ortholog Tb927.3.1990 (XP_843793.1), namely TbTTC29 in this study, which shares 22% of identity (40% of similarity) with the human ortholog. TbTTC29 is a 481 amino-acids protein and annotated as a Tetratricopeptide repeat putative protein. We generated a trypanosome cell line expressing a tagged version of the endogenous TbTTC29 protein, *TbTTC29::TY1* and investigated the protein localization by immunofluorescence on detergent-extracted cytoskeleton preparations (CSK) (**Figure 5, Figure S10**). *TbTTC29::TY1* was found to localise to the flagellum with

staining adjoined to that of the paraflagellar rod protein PFR2. In addition, *TbTTC29::TY1* was labelled at both the old flagellum (OF) and the new flagellum (NF), even when the later has not assembled a PFR structure yet. Our data therefore indicate that *TbTTC29::TY1* is an axonemal-associated protein, which localises along the axoneme from the transition zone, specifically labelled with anti-FTZC⁵⁶ to the distal tip (**Figure 5**).

Phenotypical characterization of *TbTTC29* RNAi-knockdown

To assess the functional role of *TbTTC29* in the parasite, we used the tetracycline-inducible RNA interference (RNAi) system. We generated an RNAi inducible *TbTTC29::TY1*/RNAi^{*TbTTC29*} cell line by targeting nucleotides 352 to 806 of the transcript sequence. Induction of the RNAi led to a substantial reduction of *TbTTC29::TY1* expression, as demonstrated by western blotting analysis (**Figure 6A insert**). Functional analysis of RNAi induced cells showed that *TbTTC29* knockdown did not dramatically affect the growth rate nor the morphology of the cells, in comparison with non-induced or parental cells (**Figure 6A**). In addition, when performing TEM analysis, the flagella appeared normal in number, length and their overall structure was preserved (data not shown). However, we observed that RNAi induced cells were more prone to sediment in comparison to non-induced cells (**Figure 6B**). Hence, quantitative sedimentation assays indicated that following 120 hours of tetracycline treatment, 70% of the RNAi induced cells had sedimented compared to 30% for the non-induced cells. Such an increase in sedimentation is directly correlated to defects in flagellar motility and cell mobility, which we confirmed by video microscopy (**movies S1 and S2**) and mobility tracking (**Figure 6F**). Overall, this functional study demonstrated that in *T. brucei*, similar to what we observed in the mice and in humans, the *TTC29* protein is involved in flagellar beating and motility.

Determination of the protein region required for localization and function of TTC29 protein in *T. brucei*

Based on the functional similarity observed between HsTTC29, MmusTTC29 and TbTTC29, we decided to further utilise the *T. brucei* model in order to investigate the role of the TPR domains in TTC29 protein localization and function. We generated a construct encoding the N-terminus domain of TbTTC29 protein (amino acids 1-120) and lacking the TPR repeats, *TbTTC29-Nter::myc*, which was expressed in the *TbTTC29::TY1/ RNAi^{TbTTC29}* background cell line; thus generating the cell line *TbTTC29::TY1/TbTTC29-Nter::myc/RNAi^{TbTTC29}*. In this cell line the RNAi was designed to specifically target the full-length *TbTTC29* protein with the N-terminus construct, therefore, being not affected. The endogenous expression level of *TbTTC29-Nter::myc* did not further affect the cell growth (**Figure 6C**); the slight growth delay observed during induction of *RNAi^{TbTTC29}* was found to persist. However, in contrast to *TbTTC29::TY1* that was detected in the whole cell (WC), the detergent-extracted cell (cytoskeleton, CSK), and the flagellum (FG) fractions by means of western-blotting, the *TbTTC29-Nter::myc* protein was only detected in the WC fraction (**Figure 6D**), therefore indicating that the N-terminus domain is not sufficient to position the protein within the axoneme. This was further confirmed by immunodetection of *TbTTC29-Nter::myc*, which showed its localization within the cytoplasm of non-extracted cells but not in the flagellum from detergent-extracted cytoskeleton preparations (**Figure 6E, Figure S10**). Importantly, expression of *TbTTC29-Nter::myc* could not rescue the sedimentation phenotype induced by *TbTTC29* RNAi knockdown, as shown in **Figure 6B**. Taken together, these experiments demonstrate that the TPR domains located in the second half of the TTC29 protein are required for proper localization of the protein into the axoneme and proper function in flagella beating and motility.

Structural analysis of *HsTTC29*, *MmusTTC29* and *TbTTC29* proteins

High preference for α -helicity in HsTTC29 protein can be predicted on the basis of its primary sequence, with only four strong helix-forming residues (Alanine, Glutamic acid, Histidine and Leucine) accounting for a third of all residues^{57; 58}. In fact, five tandem helical repeats were initially identified as TPR domains using SMART prediction software (aa 182-215, 234-267, 274-307, 314-347, 354-387) (**Figure 1**). As SMART analysis is only based on primary sequence and may provide incomplete information on structural motifs, we performed a secondary structure prediction⁵⁹ followed by manual alignment of suspect peptides⁴¹. By doing that, we identified 7 pairs of helices (36-40 amino-acids) compactly disposed throughout the central part of the protein sequence, flanked by unpaired N-terminal and C-terminal helices. On the basis of significant conservation both within and outside of the consensus TPR sites (4, 7, 8, 11, 20, 24, 27 and 32)⁴¹, we hypothesize that HsTTC29 contains up to 7 TPRs, which are stabilized by additional helices that have been referred to as ‘capping’ or ‘solubilization’ helices in the context of TPR proteins⁶⁰ (**Figure S11A**). The N-terminal repeat 1 and 2, featuring non-canonical residues at the key 8 and 20 positions (e.g., F104 instead of G/A/S, K117 and R159 instead of A/S/E), were not recognized by SMART as TPRs. However, the peculiar helical pairing and significant conservation outside of the consensus sites make us hypothesize that these regions fold into TPR-like structures. Furthermore, an attempt to identify a suitable template for creating a homology model of HsTTC29, yields an adaptor LGN protein involved in spindle orientation (e.g., PDB ID 6HC2) at 18% sequence identity, which features 8 compactly disposed TPRs with similar poor consensus retention at the N-terminal repeat⁶¹, thus confirming the identified TPR domains in HsTTC29. In MsTTC29, which shares 75% of identity (85% of similarity) with HsTTC29, 7 TPR domains were similarly identified. In TbTTC29, the N-terminal TPR was found severely truncated in the middle of the sequence, although some sequence conservation

with the corresponding segments in human and murine orthologs persists (**Figure S11B**). Overall, as illustrated in Figure S9B, HsTTC29, MmusTTC29 and TbTTC29 proteins display a significant level of conservation, particularly within the TPR regions internal to the protein, suggesting that in mammals and *T. brucei*, the TPR domains are likely to be critical for localization and function of TTC29 orthologs. The compact and extended nature of the TPR repeats in these proteins also indicates their ability to participate in protein–protein interactions via concave amphipathic super-helical structures; such repeats are known to self-assemble⁶², which is likely, responsible for functional roles displayed by these proteins.

Discussion

We report here the identification of bi-allelic mutations in *TTC29* inducing a MMAF phenotype, asthenozoospermia and sterility in men. *TTC29*₂ and *TTC29*₃ individuals were born from related parents (2nd and 1st degree cousins respectively) but familial information was not available for the other three individuals. The presence of the described *TTC29* homozygous truncating variants in five seemingly unrelated individuals is highly suggestive of recessive inheritance. Unfortunately, we could not test any other family member's to obtain additional genotype-phenotype correlation. However, all affected men were conceived spontaneously from very likely heterozygous fathers (and mothers) and the five mutated subjects had at least one sibling. This constitutes strong indirect evidence that men carrying a heterozygous *TTC29* truncating variant are fertile, and that *TTC29* associated MMAF is transmitted under a recessive mode of inheritance. Importantly, by analyzing *TTC29* orthologs in the mouse and in the flagellated parasite *T. brucei*, we provide further demonstration of the importance of *TTC29* proteins in flagellar beating and motility. We show that *TTC29* mutations identified in the five infertile individuals result in the total absence of the protein or at best to truncated proteins lacking the critical TPR region. We

demonstrated that this TPR region is important for TTC29 localization and function in *T. brucei*, by using a truncated TbTTC29 protein, which failed to locate to the axoneme and to rescue the cell mobility defects induced by silencing the endogenous *TbTTC29* expression.

To date, the precise function of TTC29 in humans and the details of its molecular interactions are unknown, but it is very likely that similar to *T. brucei*, the TPRs are important for TTC29 function in human sperm. TPR motifs are usually found in arrays of 2 to 20 repeats, which provide coiled and super-helical structures for protein interactions. The TPR-containing (TTC) proteins are widely present from bacteria to humans and are involved in various important biological processes, such as intracellular transport, vesicle fusion, protein folding, cell cycle, and transcriptional regulation⁴⁰. By performing *in silico* structural analyses and alignment of human, mouse and trypanosome TTC29 protein, we provide a better characterization of TPR structural domains in human TTC29 protein and confirmed the high conservation of such domains in mouse and trypanosome. Most importantly, we identify TTC29 homology with LGN, which was described to associate with cytoplasmic dynein/dynactin that positions the spindle microtubules during cell division⁶³. Such similarity is in favor of a possible function of TTC29 in the transport and/or positioning of microtubules and axonemal proteins.

Interestingly, TTC proteins were described to be enriched in the Intra Flagellar Transport (IFT) and the BBSome complexes, both being critical for cilia and flagella assembly⁶⁴⁻⁶⁷. Accordingly, in humans, some *TTC* loss of function mutations were described to induce defects in ciliary structure and function^{68; 69}. In addition, recent work from Liu et al, reported the identification of MMAF infertile individuals with truncating mutations in *TTC21A* (MIM 611430), also known as *IFT139A*, encoding for an IFT-A subcomplex protein²⁷. So far, no experimental evidences indicating that TTC29 is part of IFT complexes have been reported in humans but *in silico* prediction software (String) identified TTC29 in

the functional association network including TTC26 and TTC30A/B, two known components of the anterograde IFT-B complex. In line with these elements, work from Cheung et al identified *Ttc29* in *Xenopus* as a direct target of RFX2, a transcription factor coordinating ciliogenesis and demonstrated that *Ttc29* knockdown in multi-ciliated epithelial cells of *Xenopus*, strongly impacted the size and number of cilia, indicating that TTC29 was part of the IFT-B complex⁷⁰. Taken together, these results suggest that in humans, the function of TTC29 is likely to be related to IFT, in line with the MMAF phenotype observed in individuals carrying *TTC29* truncating mutations. The situation in the mouse and in *T. brucei* seems to be slightly different as the observed morphological and ultra-structural defects were less severe than in human although flagellar beating and motility were profoundly impaired. Interestingly, in *Leishmania*, deletion of TTC29 induced both shortening of the flagellum and motility defect⁷¹. In keeping with TTC29 possible function in IFT, these observations would suggest a partial functional compensation of TTC29 deficiency in mouse and in the parasite. In this regard, our observation that the sperm parameters and axonemal defects of individuals carrying mutations in *TTC29* were less severe than those observed in individuals carrying mutations in two other MMAF-related genes, *CFP43* and *CFPA44*, is stimulating as it could relate to similar redundancy in human TTC protein function.

Another essential point concerns the motility and flagellar beating defects, which constitute a shared phenotype in the three studied models. All *TTC29* mutated individuals presented zero progressive motility, and the flagellar beating was profoundly impacted in the mouse and in *T. brucei*, precluding cell progression. This could be due to a direct consequence of the IFT defect, impacting the composition and functionality of protein complexes involved in beating activity and/or regulation. It also raises the hypothesis that in addition to structural function mediated through IFT, the TTC29 protein could also fulfill some specific functions required for flagellar beating itself. In line with this later hypothesis,

studies performed in *Chlamydomonas*, previously reported that the TTC29 ortholog, called p44, is a component of IDAs³¹. TTC29 may therefore be directly involved in the dynein complexes, which are well-established as critical protein complexes orchestrating the beating of cilia and flagella.

Overall, the combination of our data obtained in human, mouse and *T. brucei* are consistent with a function of TTC29 in IFT and flagellar beating, in line with previously published data regarding TTC29 orthologs localization and function in *Xenopus* and *Chlamydomonas*, respectively. Further studies using those evolutionary-distant and complementary study-models should help in precisely defining the molecular mechanisms underlying TTC29 function in flagella assembly and beating.

References

1. Satir, P., and Christensen, S.T. (2007). Overview of structure and function of mammalian cilia. *Annual review of physiology* 69, 377-400.
2. Ishikawa, T. (2017). Axoneme Structure from Motile Cilia. *Cold Spring Harb Perspect Biol* 9.
3. Holstein, A.F.C., Roosen Runge, E.C. (1981). *Atlas of Human Spermatogenesis*.(Berlin: Grosse Verlag).
4. Eddy, E.M., Toshimori, K., and O'Brien, D.A. (2003). Fibrous sheath of mammalian spermatozoa. *Microsc Res Tech* 61, 103-115.
5. Ferramosca, A., and Zara, V. (2014). Bioenergetics of mammalian sperm capacitation. *Biomed Res Int* 2014, 902953.
6. Cooper, T.G., Noonan, E., von Eckardstein, S., Auger, J., Baker, H.W., Behre, H.M., Haugen, T.B., Kruger, T., Wang, C., Mbizvo, M.T., et al. (2010). World Health Organization reference values for human semen characteristics. *Human reproduction update* 16, 231-245.
7. Bisgrove, B.W., and Yost, H.J. (2006). The roles of cilia in developmental disorders and disease. *Development* 133, 4131-4143.
8. Mitchison, H.M., and Valente, E.M. (2017). Motile and non-motile cilia in human pathology: from function to phenotypes. *J Pathol* 241, 294-309.
9. Curi, S.M., Ariagno, J.I., Chenlo, P.H., Mendeluk, G.R., Pugliese, M.N., Sardi Segovia, L.M., Repetto, H.E., and Blanco, A.M. (2003). Asthenozoospermia: analysis of a large population. *Arch Androl* 49, 343-349.

10. Chemes, H.E., Brugo, S., Zanchetti, F., Carrere, C., and Lavieri, J.C. (1987). Dysplasia of the fibrous sheath: an ultrastructural defect of human spermatozoa associated with sperm immotility and primary sterility. *Fertil Steril* 48, 664-669.
11. Escalier, D. (2006). Arrest of flagellum morphogenesis with fibrous sheath immaturity of human spermatozoa. *Andrologia* 38, 54-60.
12. Ray, P.F., Toure, A., Metzler-Guillemain, C., Mitchell, M.J., Arnoult, C., and Coutton, C. (2017). Genetic abnormalities leading to qualitative defects of sperm morphology or function. *Clin Genet* 91, 217-232.
13. Auger, J., Jouannet, P., and Eustache, F. (2016). Another look at human sperm morphology. *Hum Reprod* 31, 10-23.
14. Ben Khelifa, M., Coutton, C., Zouari, R., Karaouzene, T., Rendu, J., Bidart, M., Yassine, S., Pierre, V., Delaroche, J., Hennebicq, S., et al. (2014). Mutations in DNAH1, which encodes an inner arm heavy chain dynein, lead to male infertility from multiple morphological abnormalities of the sperm flagella. *Am J Hum Genet* 94, 95-104.
15. Sha, Y., Yang, X., Mei, L., Ji, Z., Wang, X., Ding, L., Li, P., and Yang, S. (2017). DNAH1 gene mutations and their potential association with dysplasia of the sperm fibrous sheath and infertility in the Han Chinese population. *Fertil Steril* 107, 1312-1318 e1312.
16. Wang, X., Jin, H., Han, F., Cui, Y., Chen, J., Yang, C., Zhu, P., Wang, W., Jiao, G., Wang, W., et al. (2017). Homozygous DNAH1 frameshift mutation causes multiple morphological anomalies of the sperm flagella in Chinese. *Clin Genet* 91, 313-321.
17. Li, Y., Sha, Y., Wang, X., Ding, L., Liu, W., Ji, Z., Mei, L., Huang, X., Lin, S., Kong, S., et al. (2019). DNAH2 is a novel candidate gene associated with multiple morphological abnormalities of the sperm flagella. *Clin Genet* 95, 590-600.
18. Coutton, C., Vargas, A.S., Amiri-Yekta, A., Kherraf, Z.E., Ben Mustapha, S.F., Le Tanno, P., Wambergue-Legrand, C., Karaouzene, T., Martinez, G., Crouzy, S., et al. (2018). Mutations in CFAP43 and CFAP44 cause male infertility and flagellum defects in *Trypanosoma* and human. *Nat Commun* 9, 686.
19. Tang, S., Wang, X., Li, W., Yang, X., Li, Z., Liu, W., Li, C., Zhu, Z., Wang, L., Wang, J., et al. (2017). Biallelic Mutations in CFAP43 and CFAP44 Cause Male Infertility with Multiple Morphological Abnormalities of the Sperm Flagella. *Am J Hum Genet* 100, 854-864.
20. Wu, H., Li, W., He, X., Liu, C., Fang, Y., Zhu, F., Jiang, H., Liu, W., Song, B., Wang, X., et al. (2019). Novel CFAP43 and CFAP44 mutations cause male infertility with multiple morphological abnormalities of the sperm flagella (MMAF). *Reprod Biomed Online* 38, 769-778.
21. Dong, F.N., Amiri-Yekta, A., Martinez, G., Saut, A., Tek, J., Stouvenel, L., Lores, P., Karaouzene, T., Thierry-Mieg, N., Satre, V., et al. (2018). Absence of CFAP69 Causes Male Infertility due to Multiple Morphological Abnormalities of the Flagella in Human and Mouse. *Am J Hum Genet* 102, 636-648.
22. Kherraf, Z.E., Amiri-Yekta, A., Dacheux, D., Karaouzene, T., Coutton, C., Christou-Kent, M., Martinez, G., Landrein, N., Le Tanno, P., Fourati Ben Mustapha, S., et al. (2018). A Homozygous Ancestral SVA-Insertion-Mediated Deletion in WDR66 Induces Multiple Morphological Abnormalities of the Sperm Flagellum and Male Infertility. *Am J Hum Genet* 103, 400-412.
23. Auguste, Y., Delague, V., Desvignes, J.P., Longepied, G., Gnisci, A., Besnier, P., Levy, N., Beroud, C., Megarbane, A., Metzler-Guillemain, C., et al. (2018). Loss of Calmodulin- and Radial-Spoke-Associated Complex Protein CFAP251 Leads to Immotile Spermatozoa Lacking Mitochondria and Infertility in Men. *Am J Hum Genet* 103, 413-420.

24. Martinez, G., Kherraf, Z.E., Zouari, R., Fourati Ben Mustapha, S., Saut, A., Pernet-Gallay, K., Bertrand, A., Bidart, M., Hograindleur, J.P., Amiri-Yekta, A., et al. (2018). Whole-exome sequencing identifies mutations in FSIP2 as a recurrent cause of multiple morphological abnormalities of the sperm flagella. *Hum Reprod* 33, 1973-1984.
25. Coutton, C., Martinez, G., Kherraf, Z.E., Amiri-Yekta, A., Boguenet, M., Saut, A., He, X., Zhang, F., Cristou-Kent, M., Escoffier, J., et al. (2019). Bi-allelic Mutations in ARMC2 Lead to Severe Astheno-Teratozoospermia Due to Sperm Flagellum Malformations in Humans and Mice. *Am J Hum Genet* 104, 331-340.
26. Shen, Y., Zhang, F., Li, F., Jiang, X., Yang, Y., Li, X., Li, W., Wang, X., Cheng, J., Liu, M., et al. (2019). Loss-of-function mutations in QRICH2 cause male infertility with multiple morphological abnormalities of the sperm flagella. *Nat Commun* 10, 433.
27. Liu, W., He, X., Yang, S., Zouari, R., Wang, J., Wu, H., Kherraf, Z.E., Liu, C., Coutton, C., Zhao, R., et al. (2019). Bi-allelic Mutations in TTC21A Induce Asthenoteratospermia in Humans and Mice. *Am J Hum Genet* 104, 738-748.
28. Liu, C., Lv, M., He, X., Zhu, Y., Amiri-Yekta, A., Li, W., Wu, H., Kherraf, Z.E., Liu, W., Zhang, J., et al. (2019). Homozygous mutations in SPEF2 induce multiple morphological abnormalities of the sperm flagella and male infertility. *J Med Genet*.
29. Sha, Y.W., Xu, X., Mei, L.B., Li, P., Su, Z.Y., He, X.Q., and Li, L. (2017). A homozygous CEP135 mutation is associated with multiple morphological abnormalities of the sperm flagella (MMAF). *Gene* 633, 48-53.
30. Lores, P., Coutton, C., El Khouri, E., Stouvenel, L., Givelet, M., Thomas, L., Rode, B., Schmitt, A., Louis, B., Sakheli, Z., et al. (2018). Homozygous missense mutation L673P in adenylate kinase 7 (AK7) leads to primary male infertility and multiple morphological anomalies of the flagella but not to primary ciliary dyskinesia. *Hum Mol Genet* 27, 1196-1211.
31. Yamamoto, R., Yanagisawa, H.A., Yagi, T., and Kamiya, R. (2008). Novel 44-kilodalton subunit of axonemal Dynein conserved from chlamydomonas to mammals. *Eukaryotic cell* 7, 154-161.
32. Poon, S.K., Peacock, L., Gibson, W., Gull, K., and Kelly, S. (2012). A modular and optimized single marker system for generating *Trypanosoma brucei* cell lines expressing T7 RNA polymerase and the tetracycline repressor. *Open Biol* 2, 110037.
33. Wirtz, E., Leal, S., Ochatt, C., and Cross, G.A. (1999). A tightly regulated inducible expression system for conditional gene knock-outs and dominant-negative genetics in *Trypanosoma brucei*. *Mol Biochem Parasitol* 99, 89-101.
34. Baker, N., Alsford, S., and Horn, D. (2011). Genome-wide RNAi screens in African trypanosomes identify the nifurtimox activator NTR and the eflornithine transporter AAT6. *Mol Biochem Parasitol* 176, 55-57.
35. Bastin, P., Bagherzadeh, Z., Matthews, K.R., and Gull, K. (1996). A novel epitope tag system to study protein targeting and organelle biogenesis in *Trypanosoma brucei*. *Mol Biochem Parasitol* 77, 235-239.
36. Florimond, C., Sahin, A., Vidilaseris, K., Dong, G., Landrein, N., Dacheux, D., Albisetti, A., Byard, E.H., Bonhivers, M., and Robinson, D.R. (2015). BILBO1 is a scaffold protein of the flagellar pocket collar in the pathogen *Trypanosoma brucei*. *PLoS Pathog* 11, e1004654.
37. Bastin, P., Pullen, T.J., Sherwin, T., and Gull, K. (1999). Protein transport and flagellum assembly dynamics revealed by analysis of the paralysed trypanosome mutant *snl-1*. *J Cell Sci* 112 (Pt 21), 3769-3777.

38. Oberholzer, M., Lopez, M.A., Ralston, K.S., and Hill, K.L. (2009). Approaches for functional analysis of flagellar proteins in African trypanosomes. *Methods Cell Biol* 93, 21-57.
39. Perez-Riba, A., and Itzhaki, L.S. (2019). The tetratricopeptide-repeat motif is a versatile platform that enables diverse modes of molecular recognition. *Curr Opin Struct Biol* 54, 43-49.
40. Zeytuni, N., and Zarivach, R. (2012). Structural and functional discussion of the tetratricopeptide repeat, a protein interaction module. *Structure* 20, 397-405.
41. Blatch, G.L., and Lassle, M. (1999). The tetratricopeptide repeat: a structural motif mediating protein-protein interactions. *BioEssays : news and reviews in molecular, cellular and developmental biology* 21, 932-939.
42. Darde, T.A., Lecluze, E., Lardenois, A., Stevant, I., Alary, N., Tuttelmann, F., Collin, O., Nef, S., Jegou, B., Rolland, A.D., et al. (2019). The ReproGenomics Viewer: a multi-omics and cross-species resource compatible with single-cell studies for the reproductive science community. *Bioinformatics*.
43. Darde, T.A., Sallou, O., Becker, E., Evrard, B., Monjeaud, C., Le Bras, Y., Jegou, B., Collin, O., Rolland, A.D., and Chalmel, F. (2015). The ReproGenomics Viewer: an integrative cross-species toolbox for the reproductive science community. *Nucleic Acids Res* 43, W109-116.
44. Wang, G., Guo, Y., Zhou, T., Shi, X., Yu, J., Yang, Y., Wu, Y., Wang, J., Liu, M., Chen, X., et al. (2013). In-depth proteomic analysis of the human sperm reveals complex protein compositions. *J Proteomics* 79, 114-122.
45. Blackburn, K., Bustamante-Marin, X., Yin, W., Goshe, M.B., and Ostrowski, L.E. (2017). Quantitative Proteomic Analysis of Human Airway Cilia Identifies Previously Uncharacterized Proteins of High Abundance. *J Proteome Res* 16, 1579-1592.
46. Ohta, M., Ohyama, K., Asano, A., Yokota, S., Khalid, A.M., and Yamano, Y. (2012). Regulation of rat tetratricopeptide repeat domain 29 gene expression by follicle-stimulating hormone. *Bioscience, biotechnology, and biochemistry* 76, 1540-1543.
47. Hashemitabar, M., Sabbagh, S., Orazizadeh, M., Ghadiri, A., and Bahmanzadeh, M. (2015). A proteomic analysis on human sperm tail: comparison between normozoospermia and asthenozoospermia. *J Assist Reprod Genet* 32, 853-863.
48. Vincensini, L., Blisnick, T., and Bastin, P. (2011). 1001 model organisms to study cilia and flagella. *Biology of the cell / under the auspices of the European Cell Biology Organization* 103, 109-130.
49. de Souza, W., and Souto-Padron, T. (1980). The paraxial structure of the flagellum of trypanosomatidae. *J Parasitol* 66, 229-236.
50. Bastin, P., Sherwin, T., and Gull, K. (1998). Paraflagellar rod is vital for trypanosome motility. *Nature* 391, 548.
51. Santrich, C., Moore, L., Sherwin, T., Bastin, P., Brokaw, C., Gull, K., and LeBowitz, J.H. (1997). A motility function for the paraflagellar rod of *Leishmania* parasites revealed by PFR-2 gene knockouts. *Mol Biochem Parasitol* 90, 95-109.
52. Pullen, T.J., Ginger, M.L., Gaskell, S.J., and Gull, K. (2004). Protein targeting of an unusual, evolutionarily conserved adenylate kinase to a eukaryotic flagellum. *Mol Biol Cell* 15, 3257-3265.
53. Ridgley, E., Webster, P., Patton, C., and Ruben, L. (2000). Calmodulin-binding properties of the paraflagellar rod complex from *Trypanosoma brucei*. *Mol Biochem Parasitol* 109, 195-201.
54. Oberholzer, M., Marti, G., Baresic, M., Kunz, S., Hemphill, A., and Seebeck, T. (2007). The *Trypanosoma brucei* cAMP phosphodiesterases TbrPDEB1 and TbrPDEB2: flagellar enzymes that are essential for parasite virulence. *Faseb J* 21, 720-731.

55. Aslett, M., Aurrecochea, C., Berriman, M., Brestelli, J., Brunk, B.P., Carrington, M., Depledge, D.P., Fischer, S., Gajria, B., Gao, X., et al. (2010). TriTrypDB: a functional genomic resource for the Trypanosomatidae. *Nucleic Acids Res* 38, D457-462.
56. Bringaud, F., Robinson, D.R., Barradeau, S., Biteau, N., Baltz, D., and Baltz, T. (2000). Characterization and disruption of a new *Trypanosoma brucei* repetitive flagellum protein, using double-stranded RNA inhibition. *Mol Biochem Parasitol* 111, 283-297.
57. Chou, P.Y., and Fasman, G.D. (1978). Empirical predictions of protein conformation. *Annu Rev Biochem* 47, 251-276.
58. Costantini, S., Colonna, G., and Facchiano, A.M. (2006). Amino acid propensities for secondary structures are influenced by the protein structural class. *Biochem Biophys Res Commun* 342, 441-451.
59. Drozdetskiy, A., Cole, C., Procter, J., and Barton, G.J. (2015). JPred4: a protein secondary structure prediction server. *Nucleic Acids Res* 43, W389-394.
60. D'Andrea, L.D., and Regan, L. (2003). TPR proteins: the versatile helix. *Trends Biochem Sci* 28, 655-662.
61. Takayanagi, H., Yuzawa, S., and Sumimoto, H. (2015). Structural basis for the recognition of the scaffold protein Frmpd4/Preso1 by the TPR domain of the adaptor protein LGN. *Acta Crystallogr F Struct Biol Commun* 71, 175-183.
62. Yuzawa, S., Kamakura, S., Iwakiri, Y., Hayase, J., and Sumimoto, H. (2011). Structural basis for interaction between the conserved cell polarity proteins Inscuteable and Leu-Gly-Asn repeat-enriched protein (LGN). *Proc Natl Acad Sci U S A* 108, 19210-19215.
63. Pirovano, L., Culurgioni, S., Carminati, M., Alfieri, A., Monzani, S., Cecatiello, V., Gaddoni, C., Rizzelli, F., Foadi, J., Pasqualato, S., et al. (2019). Hexameric NuMA:LGN structures promote multivalent interactions required for planar epithelial divisions. *Nat Commun* 10, 2208.
64. Xu, Y., Cao, J., Huang, S., Feng, D., Zhang, W., Zhu, X., and Yan, X. (2015). Characterization of tetratricopeptide repeat-containing proteins critical for cilia formation and function. *PLoS One* 10, e0124378.
65. Pazour, G.J., Dickert, B.L., Vucica, Y., Seeley, E.S., Rosenbaum, J.L., Witman, G.B., and Cole, D.G. (2000). *Chlamydomonas* IFT88 and its mouse homologue, polycystic kidney disease gene *tg737*, are required for assembly of cilia and flagella. *J Cell Biol* 151, 709-718.
66. Taschner, M., Bhogaraju, S., and Lorentzen, E. (2012). Architecture and function of IFT complex proteins in ciliogenesis. *Differentiation* 83, S12-22.
67. van Dam, T.J., Townsend, M.J., Turk, M., Schlessinger, A., Sali, A., Field, M.C., and Huynen, M.A. (2013). Evolution of modular intraflagellar transport from a coatomer-like progenitor. *Proc Natl Acad Sci U S A* 110, 6943-6948.
68. Tadenev, A.L., Kulaga, H.M., May-Simera, H.L., Kelley, M.W., Katsanis, N., and Reed, R.R. (2011). Loss of Bardet-Biedl syndrome protein-8 (BBS8) perturbs olfactory function, protein localization, and axon targeting. *Proc Natl Acad Sci U S A* 108, 10320-10325.
69. Davis, E.E., Zhang, Q., Liu, Q., Diplas, B.H., Davey, L.M., Hartley, J., Stoetzel, C., Szymanska, K., Ramaswami, G., Logan, C.V., et al. (2011). TTC21B contributes both causal and modifying alleles across the ciliopathy spectrum. *Nat Genet* 43, 189-196.
70. Chung, M.I., Kwon, T., Tu, F., Brooks, E.R., Gupta, R., Meyer, M., Baker, J.C., Marcotte, E.M., and Wallingford, J.B. (2014). Coordinated genomic control of ciliogenesis and cell movement by RFX2. *eLife* 3, e01439.
71. Beneke, T., Demay, F., Hookway, E., Ashman, N., Jeffery, H., Smith, J., Valli, J., Becvar, T., Myskova, J., Lestinova, T., et al. (2019). Genetic dissection of a *Leishmania*

flagellar proteome demonstrates requirement for directional motility in sand fly infections. PLoS Pathog 15, e1007828.

ACCESSION NUMBERS

The *TTC29* variants reported in this manuscript are accessible in ClinVar with the submission number SUB6408157.

Supplemental data

Supplemental Data include 11 figures, 7 tables and 2 movies.

Acknowledgements

We thank all the individuals and their families for their cooperation, as well as all the referring physicians. We thank all the technicians from the *Service de Biologie de la Reproduction* at the Hôpital Cochin (Paris) for routine semen sample evaluation (Jacques Bras, Nathalie Chériaux, Véronique Hernandorena, Jean-Claude Cambronne and Caroline Villalon). We thank the core facilities of the Institut Cochin : Transgenesis-Homologous recombination-Cryosconservation, Cellular Imaging Facility for electron microscopy procedures, histology facility HistIM (Rachel Onifarasoaniaina) together with the 3P5 proteomic facility of the University Paris Descartes (Virginie Salnot, Cédric Broussard et Evangeline Bennana). We thank Keith Gull for the L8C4 antibody (Oxford University), Klaus Ersfeld (Bayreuth University) for the anti-myc antibody (9E10), Nicolas Biteau (Bordeaux University) for the anti-PFR2 antibody, Frédéric Bringaud (Bordeaux University) for the anti-enolase and anti-FTZC, Philippe Bastin (Institut Pasteur, Paris) for the BB2 antibody, Samuel Dean (Oxford University) for the pPOT vectors. This work was supported by the Institut National de la Santé et de la Recherche Médicale (INSERM), the Centre National de la Recherche Scientifique (CNRS), the Université Paris Descartes, the University of Bordeaux, the French National Research Agency (Grant MUCOFERTIL ANR-12-BSV1-0011-01 to AT and MB, grant MASFLAGELLA ANR-14-CE15-0002-03 to PR, AT and MB), the LabEx ParaFrap (ANR-11-LABX-0024 to DRR), the FEDER (2007-2013 'Operational Programme

for Competitiveness Factors and employment' to FG) and the Canceropole Ile de France (funding to FG).

Disclosure of interests

The authors have no conflict of interest to declare

Web Resources

BLAST, (<https://blast.ncbi.nlm.nih.gov/Blast.cgi>)

ClinVar, <https://www.ncbi.nlm.nih.gov/clinvar/>

CRISPOR, <http://crispor.tefor.net/>

EMBL EBI Expression Atlas, <https://www.ebi.ac.uk/gxa/home>

gnomAD Browser, <http://gnomad.broadinstitute.org>

GTEEx, <https://gtexportal.org>

JPred4, <http://www.compbio.dundee.ac.uk/jpred/>

MaxEntScan, http://hollywood.mit.edu/burgelab/maxent/Xmaxentscan_scoreseq.html

Online Mendelian Inheritance in Man, <https://www.omim.org>

Pdb, <http://www.rcsb.org/>

ReproGenomics Viewer, <https://rgv.genouest.org/app/#/>

Smart, <http://smart.embl-heidelberg.de/>

String, <https://string-db.org/>

Uniprot, <https://www.uniprot.org/>

FIGURE LEGENDS

Figure 1. Identification of *TTC29* mutations in five unrelated infertile men and functional consequences of the c.176 +1G>A *TTC29* variant.

(A) Illustration of Sanger sequencing data for the *TTC29* mutations identified in MMAF infertile men: individuals TTC29₁, TTC29₂ and TTC29₃ carried the c.176+1G>A homozygous mutation; individual TTC29₄ carried the c.330_334delGGAGG homozygous mutation; individual TTC29₅ carried the c.750C>A homozygous mutation. (B) Schematic representation of *TTC29* exons structure (top) and predicted protein domains (bottom), according to SMART webtool and Uniprot, with position of the three different mutations identified in the gene. *TTC29* encodes a protein of 475 amino-acids that contains five tetratricopeptide domains (blue boxes). (C) At the left, RT-PCR analysis on sperm sample from individual TTC29₁, carrying the c.176 +1G>A mutation, which indicates a reduced amount of *TTC29* transcript compared to control individual while HPRT transcript level was unaffected. At the right, electrophoregram of Sanger sequencing of the amplified transcript in sperm from individual TTC29₁, which shows an abnormal exon 4-5 boundary resulting in a premature stop codon, in comparison with control individual. (D) Western blot and immunofluorescence analyses of sperm sample from individual TTC29₁, carrying the c.176 +1G>A mutation, which both indicates the absence of *TTC29* protein compared to control individual.

Figure 2. Characterization of the sperm morphological and ultra-structural phenotype of individual TTC29₁ carrying the c.176 +1G>A mutation

(A) Schorr staining of semen smears from individual TTC29₁, carrying the c.176 +1G>A mutation, showing sperm without normally constituted flagella such as coiled flagella and flagella of irregular calibre. Scale bars represent 10µm. (B) TEM analysis of spermatozoa

from individual TTC29₁, carrying the c.176 +1G>A mutation, showing abnormal flagellum assembly with a reduced mitochondrial sheath and abnormal axonemal cross sections with a lack of the central pair. Ac: acrosome, N: nucleus, M: mitochondria, Ax: axoneme, FS: fibrous sheath. Black arrows indicate abnormal structures. Scale bars represent 1µm and 100nm. (C) Immunofluorescence staining of spermatozoa from control and individual TTC29₁, carrying the c.176 +1G>A mutation, with SPAG6 antibody (in red) and Tubulin (in green). Cells were counterstained with DAPI (blue) as nuclei marker. Scale bars represent 5µm.

Figure 3. Characterization of the sperm morphological and ultra-structural phenotype of *Ttc29*^{-/-} L5 and L7 mutant mice

(A) Papanicolaou staining of epididymal sperm from *Ttc29*^{-/-} L5 and L7 mutant mice, showing the presence of morphological abnormalities (black arrows) such as flagella bending, flagella of irregular caliber and midpiece-principal piece disjunction as compared with control sperm (WT). Scale bars represent 10µm. (B) TEM analysis of epididymal sperm from *Ttc29*^{-/-} L5 and L7 mutant mice, showing abnormal cross sections of the axoneme with ectopic peripheral doublets, lack of the central pair and global disorganization of the structure as compared to control sperm with (9+2) canonical structure (WT). Scale bars represent 100nm.

Figure 4. Characterization of sperm motility and fertilization potential of *Ttc29*^{-/-} L5 and L7 mutant mice

(A) Assessment of sperm kinematic movement of *Ttc29*^{-/-} L5 and L7 mutant mice by CASA, indicating reduced curvilinear velocity (VCL) and beat/cross frequency (BCF) as compared with controls (WT) while the amplitude of lateral head displacement (ALH) was found unaffected. Data are represented as the mean ± SEM. p-value <0.05 (*); p-value <0.01 (**);

p-value <0.001 (***) ; non-significant (ns). **(B)** *In vitro* fertilization assays with capacitated sperm from *Ttc29*^{-/-} L5 and L7 epididymes, showing reduced fertilization rates and fertilization index when inseminated with cumulus-intact oocytes and Zona-free oocytes, respectively, as compared with control sperm (WT). The total number of analyzed oocytes is indicated above the histogram of each mouse genotype. Data are represented as the mean \pm SEM. p-value <0.01 (**); p-value <0.001 (***) ; p-value <0.0001 (****). Each experiment was repeated three times. **(C)** *In vivo* breeding assays of *Ttc29*^{-/-} L5 and L7 mutant mice with wild-type females, showing a reduced number of pups per litter (left pane) and of litters per female (right panel) over a breeding period of 124 days, as compared to control males (WT). The total numbers of litters analyzed and the number of female breeders used for each genotype is indicated at the top of the histograms (left panel and right panel, respectively). Data are represented as the mean \pm SEM. p-value <0.05 (*); p-value <0.01 (**); p-value <0.001 (***) .

Figure 5. Localization of TTC29 orthologous protein, TbTTC29, in *T. brucei* flagellar axoneme.

(A) Representative picture of detergent-extracted parental cells immunolabelling, with anti-PFR (red) that labels the para-axonemal paraflagellar rod structure and anti-TY1 (green) antibodies, as a negative experimental control. **(B)** Representative picture of detergent-extracted *TbTTC29::TY1* cell line immunolabelling with anti-PFR (red) and anti-TY1 (green) antibodies, showing axonemal localization of the endogenous recombinant *TbTTC29::TY1* at both the old flagellum (OF) and the new flagellum (NF). **(C)** Representative picture detergent-extracted *TbTTC29::TY1* cell line immunolabelling with anti-FTZC labelling the transition zone (red) and anti-TY1 (green) antibodies, showing localization of *TbTTC29::TY1* from the transition zone to the distal tip of the axoneme. The mitochondrial genome and the

nuclei are stained with DAPI. Scale bars represent 5 μm in main figures and 1 μm in zoom insets. OF and NF indicated the old flagellum and the new flagellum, respectively.

Figure 6. Characterization of the cell motility phenotype induced by *TbTTC29* RNAi-induced knockdown in *T. brucei*.

(A) Comparative growth curve of parental, non-induced and RNAi-induced *TbTTC29::TY1*/RNAi^{*TbTTC29*} cells. Inset: Western-blot analysis of RNAi knockdown by immunolabelling of *TbTTC29::TY1* at 0, 72, 96, and 120 H of induction with tetracycline. Anti-enolase was used for loading normalisation. (B) Sedimentation assays at 48 and 120 hours post-RNAi^{*TbTTC29*} induction. Percentages of sedimentation were normalised to basal levels of sedimentation in the parental cells. (C) Comparative growth curves for parental, non-induced and RNAi-induced *TbTTC29::TY1*/*TbTTC29-Nter::myc*/RNAi^{*TbTTC29*} cells. (D) Western blot analysis of *TbTTC29::TY1* and *TbTTC29-Nter::myc* in protein extracts from whole cells (WC), cytoskeleton (CSK) and flagella fractions (FG), showing the presence of *TbTTC29::TY1* in all preparations while *TbTTC29-Nter::myc* is only detected in the whole cell fraction. Anti-PFR2 was used as a control for CSK and FG fractions, anti-enolase was used as a control for the cytosolic fraction. (E) Representative picture of *TbTTC29-Nter::myc* (anti-myc) and of *TbTTC29::TY1* (anti-TY1) immunolabelling on whole cells or detergent-extracted cytoskeleton preparations, showing the absence of axonemal localization for the truncated N-terminus protein. The kinetoplasts and the nuclei are stained with DAPI. Scale bars represent 5 μm . (F) Mobility graphs obtained from movies of non-induced (movie S1) and RNAi^{*TbTTC29*} (movie S2). The positions of individual cells are plotted at 0.2 s intervals. Open circle: starting position of each cell. Arrowhead: ending position. Bars represent 10 μm . In A, B and C, data are represented as the mean \pm SEM.

Movies S1 and S2. Video microscopy of WT (video S1) and RNAi^{TbTTC29} (video S2) induced cells (8 days), indicating flagellum and cell motility defects of the RNAi-induced mutant cells, which remained primarily at one location while the WT cells travelled long distances.

Table 2. Comparison of semen parameters and sperm morphological defects of individuals carrying mutations in *TTC29* (n = 5) versus other MMAF subjects of the cohort (n = 162).
 Table 1. Semen parameters and sperm morphological defects (flagellum, head and acrosome) of MMAF individuals carrying mutations in *TTC29*

	General Semen Characteristics						Flagellum defects					Head defects			Acrosome defects		
	volume (ml)	Total sperm count (10 ⁶)	Total Motility	Progressive Motility	Vitality	Typical forms	Absent	Short	Irregular	Coiled	Bent	Tapered	Thin	Micro-cephalic	Macro-cephalic	Post-acrosomal	Acrosomal
TTC29_1 <i>c.1761+G>A</i>	2.8	16.8	4	1	57	0	15	11	23	10	18	4	55	8	0	31	95
TTC29_2 <i>c.1761+G>A</i>	4	168	10	2	64	0	12	42	60	8	ND	28	12	12	0	34	60
TTC29_3 <i>c.1761+G>A</i>	4,8	91.2	7	2	65	0	30	28	46	14	0	4	4	6	2	15	98
TTC29_4 <i>c.330_334delGGAGG</i>	3	36	0	0	88	0	8	92	0	0	ND	ND	ND	ND	ND	ND	ND
TTC29_5 <i>c.750C>A</i>	6.5	38	0	0	80	0	0	90	0	0	ND	7	0	0	0	0	0
Reference limits ^a	1.5 (1.4-1.7)	39 (33-46)	40 (38-42)	32 (31-34)	58 (55-63)	23 (20-26)	5 (4-6)	1 (0-2)	2 (1-3)	17 (15-19)	13 (11-15)	3 (2-4)	14 (12-16)	7 (5-9)	1 (0-2)	42 (39-45)	60 (57-63)

Values are expressed in percent, unless specified otherwise. ND: not determined.

^a Lower and upper reference limits (5th centiles and their 95% confidence intervals) according to the World Health Organization (WHO) standards⁶ and the distribution range of morphologically abnormal spermatozoa observed in fertile individuals¹³; in bold characters: abnormal values

	General Semen Characteristics						Flagellum defects					Head defects				Acrosome defects	
	volume (ml)	Total sperm count (x10 ⁶)	Total Motility	Progressive Motility	Vitality	Typical forms	Absent	Short	Irregular	Coiled	Bent	Tapered	Thin	Micro- cephalic	Macro- cephalic	Acrosomal region*	Post-acrosomal region
<i>TTC29</i> mutated individuals	40.5 ± 3.1 (n' = 5)	70 ± 61.3 (n' = 5)	4.2 ± 4.3 (n' = 5)	1.0 ± 1.0 (n' = 5)	70.8 ± 12.7 (n' = 5)	0.0 ± 0.0 (n' = 5)	11.4 ± 12.4 (n' = 5)	52.6 ± 36.7 (n' = 5)	25.8 ± 27.0 (n' = 5)	6.4 ± 6.2 (n' = 5)	4.5 ± 9.0 (n' = 4)	10.2 ± 10.1 (n' = 5)	14.2 ± 23.3 (n' = 5)	5.2 ± 5.2 (n' = 5)	0.4 ± 0.8 (n' = 5)	63.2 ± 45.5 (n' = 4)	20.0 ± 15.7 (n' = 4)
Other MMAF individuals	40.3 ± 7.4 (n' = 116)	62.2 ± 69.4 (n' = 148)	4.6 ± 6.9 (n' = 153)	2.0 ± 4.5 (n' = 153)	56.2 ± 23.0 (n' = 150)	1.2 ± 3.2 (n' = 150)	14.9 ± 15.2 (n' = 141)	50.8 ± 29.0 (n' = 147)	26.4 ± 26.9 (n' = 142)	11.1 ± 9.9 (n' = 144)	3.7 ± 7.6 (n' = 96)	16.0 ± 17.6 (n' = 139)	6.3 ± 10.0 (n' = 136)	4.7 ± 6.6 (n' = 138)	0.6 ± 1.3 (n' = 137)	50.2 ± 37.8 (n' = 140)	20.9 ± 22.66 (n' = 136)
P value	> 0.05	> 0.05	> 0.05	> 0.05	> 0.05	> 0.05	> 0.05	> 0.05	> 0.05	> 0.05	> 0.05	> 0.05	> 0.05	> 0.05	> 0.05	> 0.05	> 0.05

Values are expressed in percent, unless specified otherwise. Values are mean ± SD; n = total number of individuals in each group; n' = number of individuals used to calculate the average based on available data. We compared statistical differences between MMAF due to *TTC29* mutations versus MMAF (multiple morphological abnormalities of the flagella) due to other known or unknown causes. Statistical analysis: Unpaired *t*-test was used to compare the two groups.

Table 3. General and sperm parameters of *TTC29*^{-/-} L5 and L7 mouse lines compared to control mice.

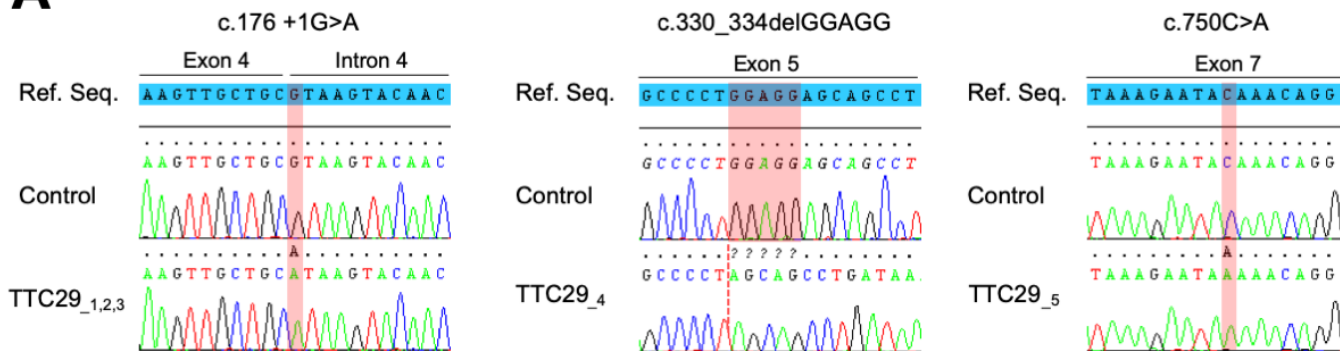
Mouse lines	Body weight (g)	Testis Weight (mg)	Apoptosis	Sperm count	Sperm Vitality (%)	Morphological defects (%)		Axonemal defects (%)
Control	27.38 ± 0.95	111.3 ± 10.8	0.34 ± 0.15	18.41 ± 1.73	48.70 ± 3.89	Head: 7.88 ± 1.79 Tail: 3.48 ± 0.59	- 2.2 ± 1.3	
KO L5	27.28 ± 0.96	93.1 ± 2.6	0.09 ± 0.02	19.33 ± 2.56	49.00 ± 2.63	Head: 6.96 ± 1.32 Tail: 7.52 ± 0.87**	- 21.6 ± 11.0 ***	
KO L7	27.38 ± 1.12	113.3 ± 14.7	0.48 ± 0.17	16.89 ± 3.72	45.45 ± 2.75	Head: 7.13 ± 1.74 Tail: 6.00 ± 0.96 *	- 13.0 ± 4.9 **	

The mean age of the animals is 4 months. Wild-type (WT mice): n=15, *Ttc29*^{-/-} L5 and L7 mice: n=10. Testis weight of each animal is pondered by mean body weight of its group; WT: n=7, *Ttc29*^{-/-} L5: n=4 and *Ttc29*^{-/-} L7: n= 5. Apoptosis rate is indicated as mean number of apoptotic cells/seminiferous tubule; WT: n=5, *Ttc29*^{-/-} L5: n=5 and *Ttc29*^{-/-} L7: n= 6. Sperm counts are indicated as mean number of sperm cells obtained from dissection of two cauda epididymes; WT: n=15, *Ttc29*^{-/-} L5 and L7: n=10. The percentage of morphological defects of the sperm head and tail is obtained by analysis of at least 100 cells for each animal on Papanicolaou-stained smears; WT: n=6, *Ttc29*^{-/-} L5: n=5 and *Ttc29*^{-/-} L7: n=4. The percentage of axonemal defects is obtained by TEM analysis of 20 to 50 axonemal cross-sections; WT: n=4, *Ttc29*^{-/-} L5: n=4 and *Ttc29*^{-/-} L7: n=3. The percentage of sperm vitality was assessed by eosine-nigrosin staining and counting of at least 200 cells per animal; WT: n=8, *Ttc29*^{-/-} L5: n=6 and *Ttc29*^{-/-} L7: n=7.

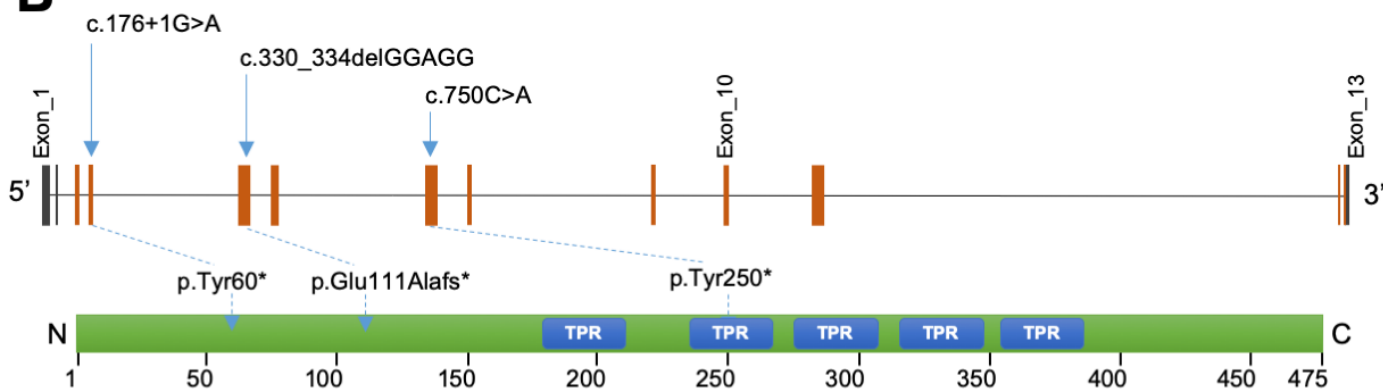
Statistical analysis: values are indicated as mean ± SEM. One-way ANOVA was used to compare the three groups, except for the analysis of the morphological defects, which was performed with a Chi-squared test (2 df). P > 0.05 was considered statistically not significant. Significant p-value are indicated as (*): p-value < 0.05, (**): p-value < 0.01 and (***): p-value < 0.001.

Figure 1

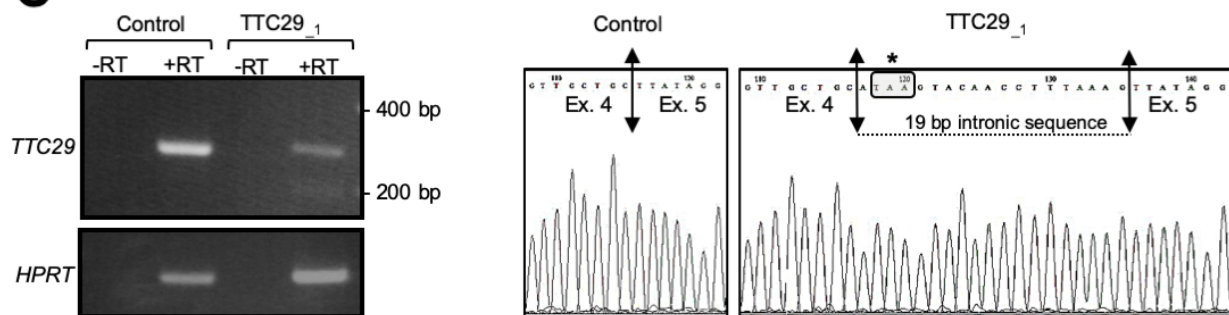
A



B



C



D

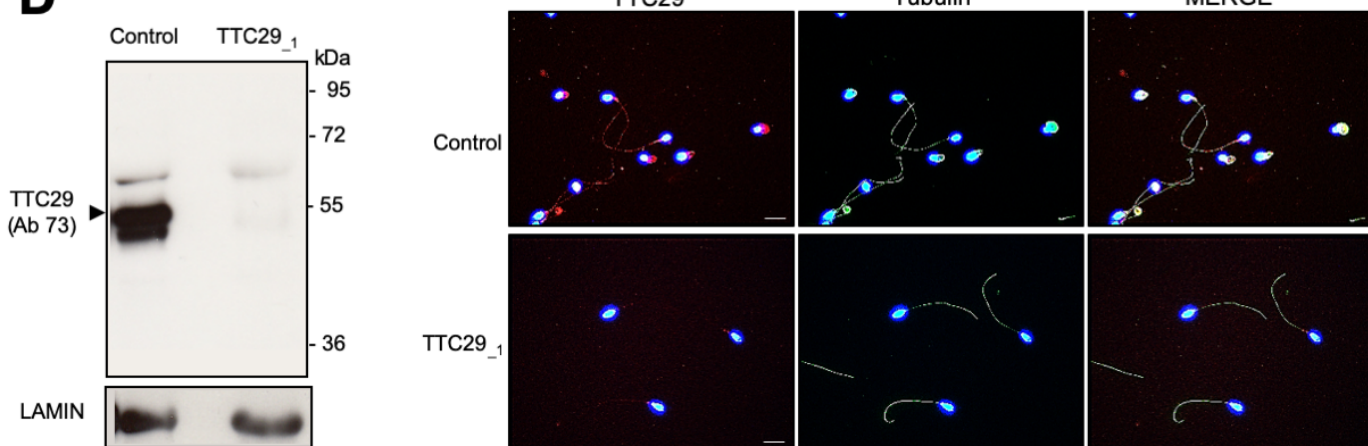


Figure 2

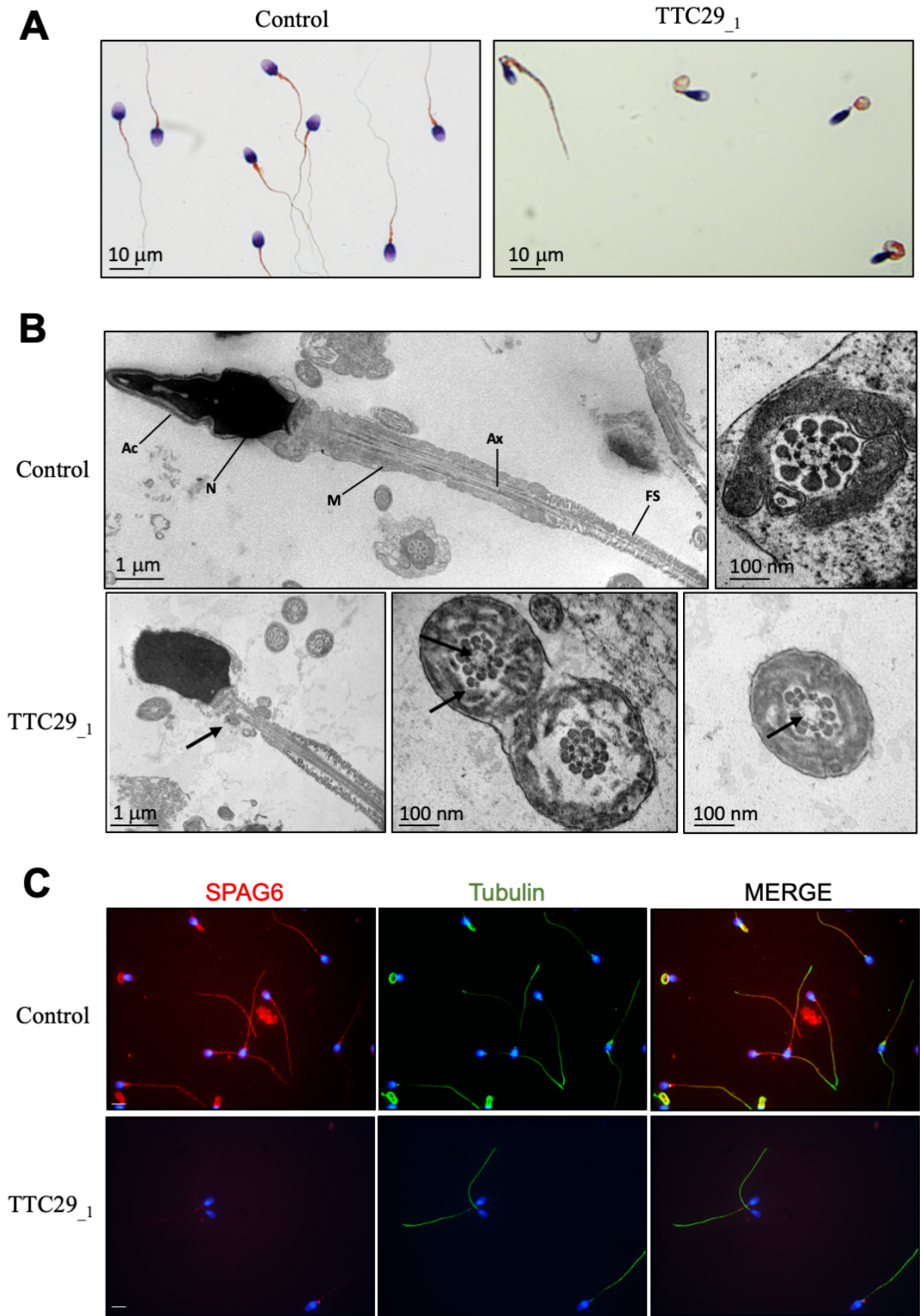
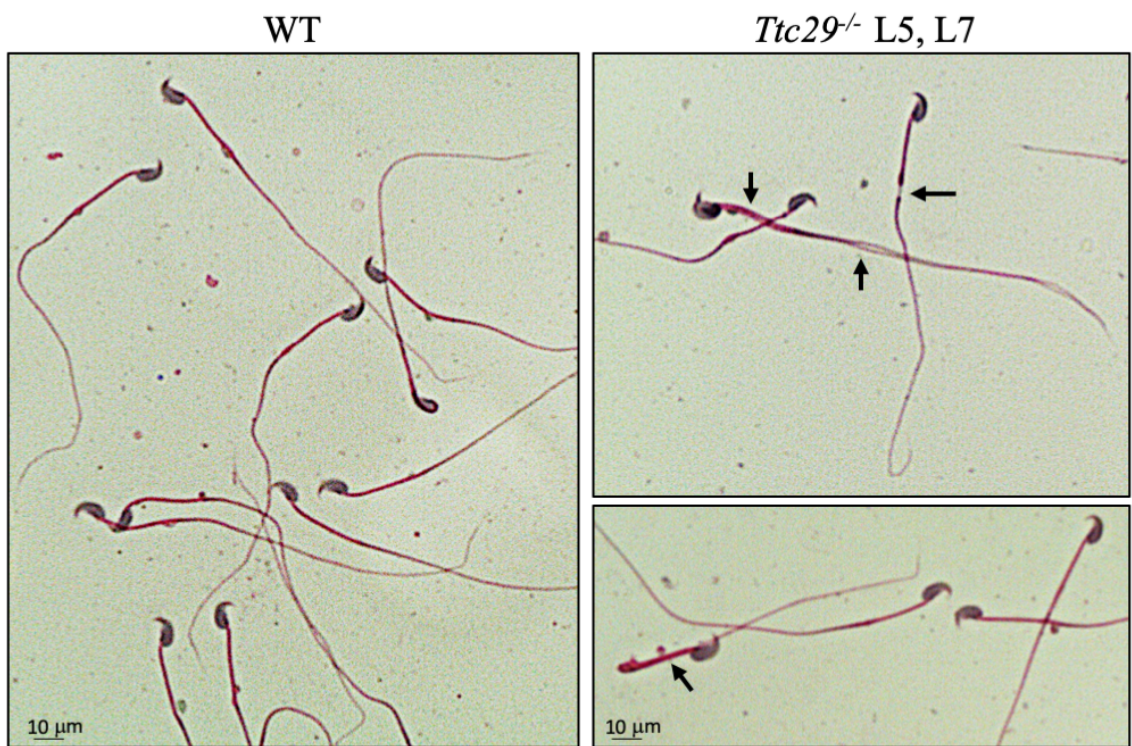


Figure 3

A



B

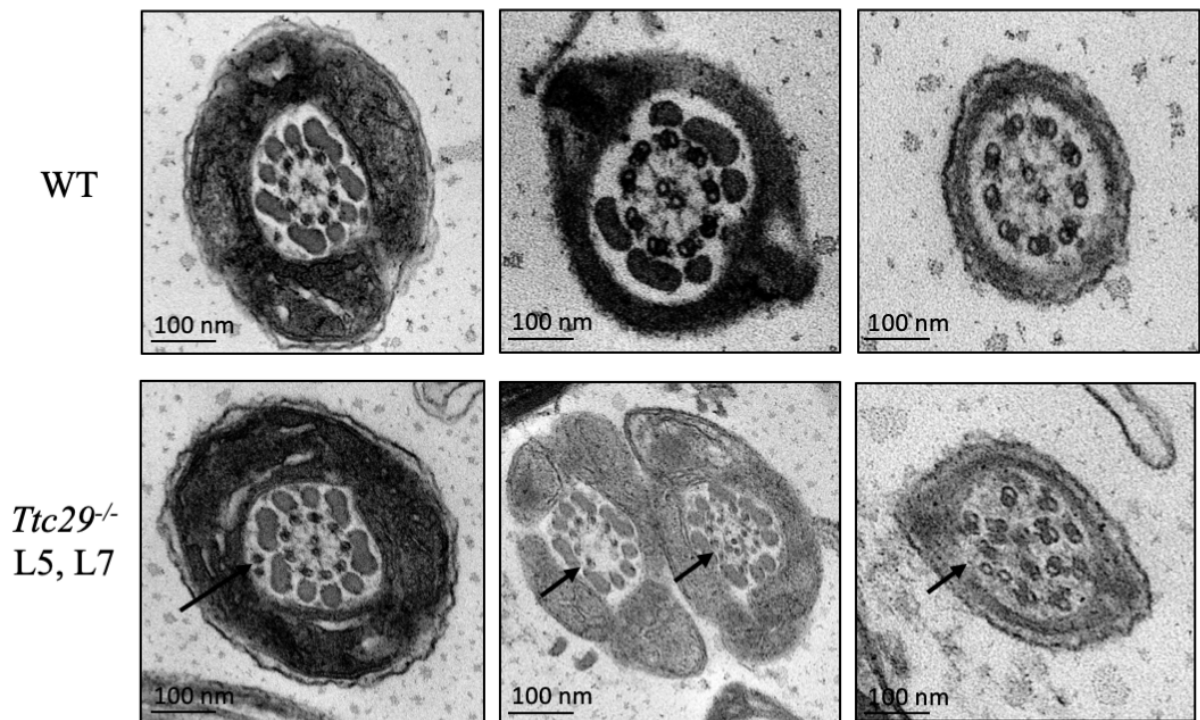
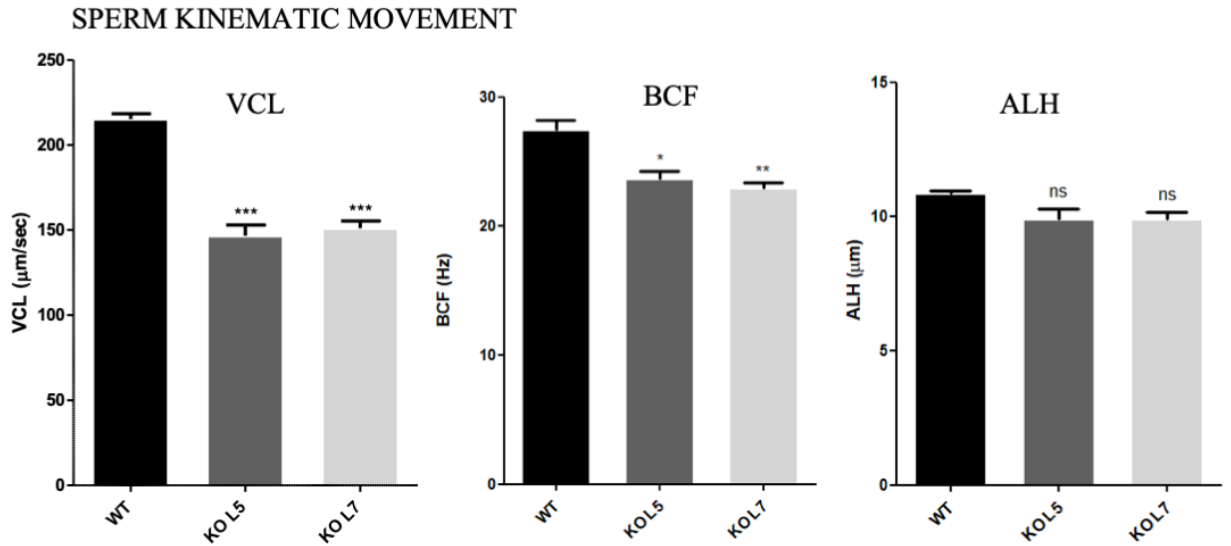
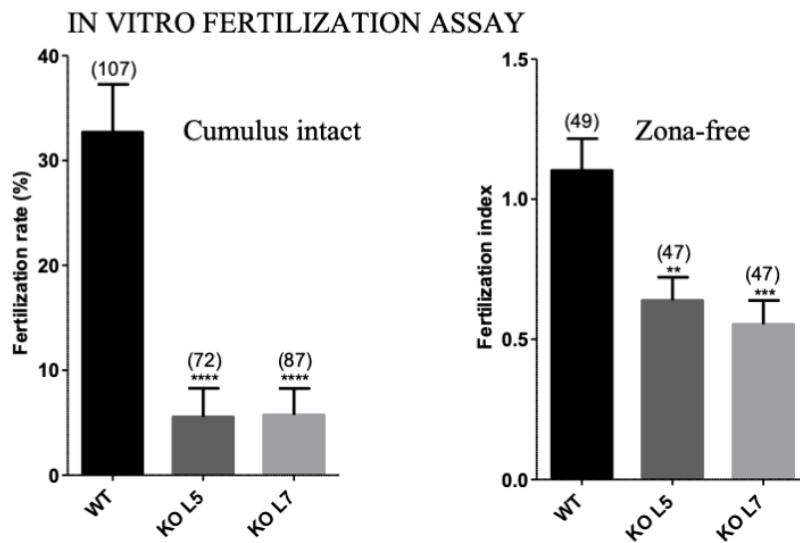


Figure 4

A



B



C

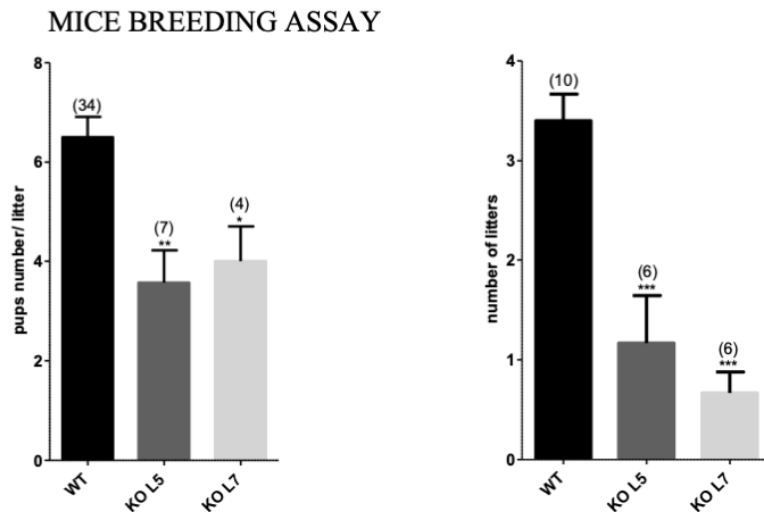


Figure 5

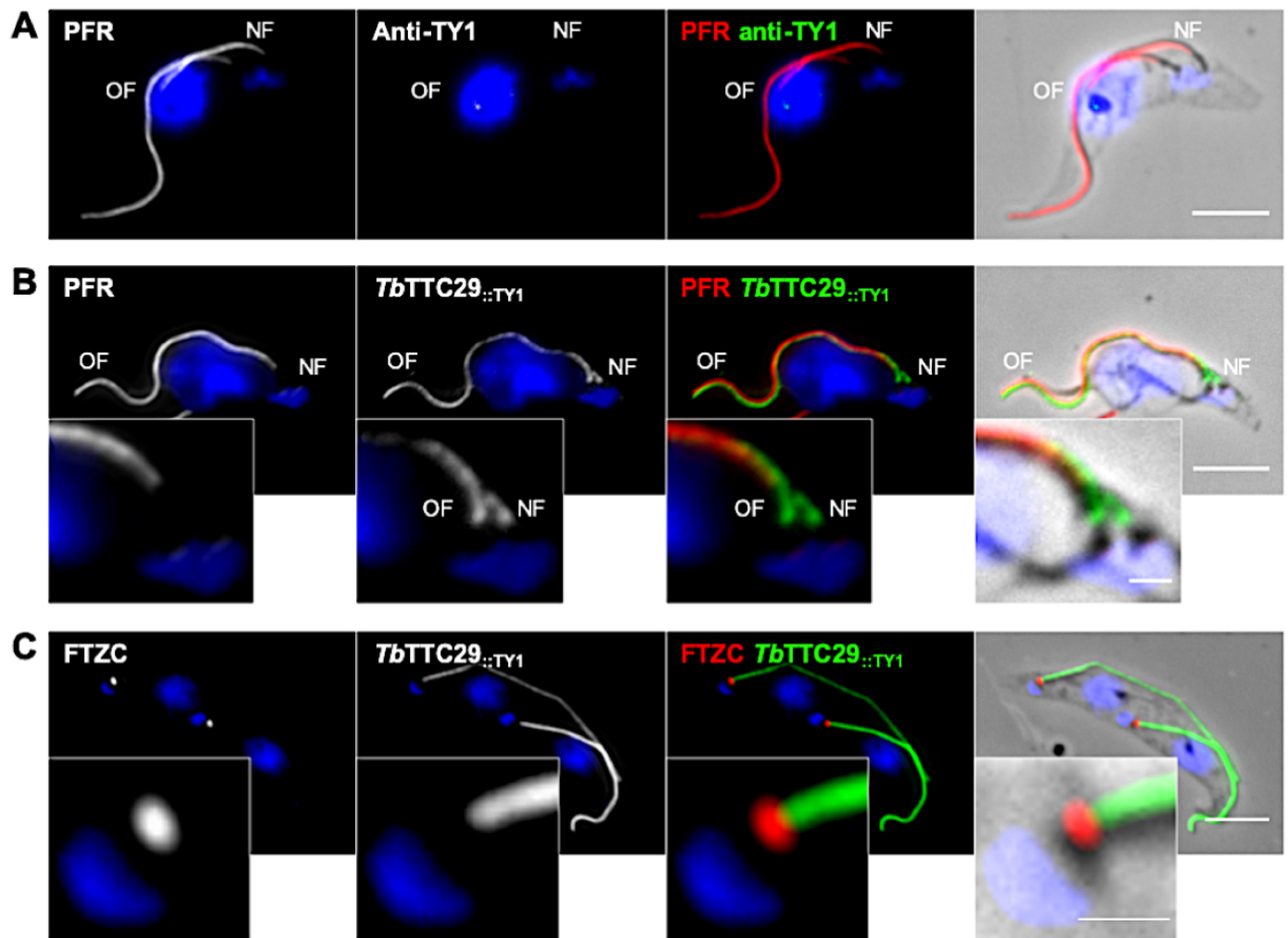


Figure 6

